Mon. Not. R. Astron. Soc. **299,** 1159–1192 (1998)

Flat-spectrum radio sources with kpc-scale structure

P. Augusto,[1,2]★ P. N. Wilkinson[1] and I. W. A. Browne[1]

[1]*Nuffield Radio Astronomy Laboratories, University of Manchester, Jodrell Bank, Macclesfield, Cheshire SK11 9DL*
[2]*Centro de Astrofísica da Universidade do Porto, Rua do Campo Alegre, 823, 4150 Porto, Portugal*

Accepted 1998 May 26. Received 1998 May 14; in original form 1998 February 27

ABSTRACT

We have carried out the first systematic study of flat-spectrum radio sources which have significant structure on angular scales 90–300 milliarcsec (mas), corresponding to linear scales of ~ 0.5–1.5 kpc at a redshift of 0.5. The principal aim of the study was to search for multiple gravitational imaging of compact radio components with image separations smaller than that of the smallest galaxy lens system known (335 mas) and corresponding to masses appropriate to compact/dwarf galaxies and to the bulges of spiral galaxies. A secondary aim was the morphological classification of a sample of flat-spectrum sources with kpc-scale structure. We particularly wanted to find out the frequency of occurrence of compact symmetric objects (CSOs: linear size < 1 kpc) and medium symmetric objects (MSOs: linear size < 15 kpc) which are believed to be the precursors of the large classical double radio sources. The parent sample consisted of 1665 flat-spectrum sources selected from two VLA surveys made with ~200 mas resolution (the Jodrell Bank–VLA Astrometric Survey – JVAS – and the Cosmic Lens All-Sky Survey – CLASS), from which we used visibility data to select sources (55 in total) with significant structure in the size range 90–300 mas. Sources with multiple compact components having a flux density ratio < 8:1 could be high-magnification lens systems, CSO/MSOs or objects with strong jets. A step-by-step observational filtering process at successively higher angular resolution was employed to classify the 55-source subsample. Initial MERLIN observations at 5 GHz (50 mas resolution) enabled us to classify ~75 per cent of the sources. The remaining sources were observed with the VLBA at 5 GHz (2 mas resolution) and in a few cases with MERLIN at 22 GHz (10 mas resolution). The resulting maps show that the majority of flat-spectrum sources with kpc-scale structure are asymmetric core–jets. The remaining sources include 23 new CSO/MSOs, a much smaller fraction of the parent sample (1.4 per cent) than is found in VLBI surveys of flat-spectrum sources (5–10 per cent). About half of the new CSO/MSOs constitute a hitherto unknown population: bright core CSO/MSOs. No definite high-magnification gravitational lenses were found. The implication is that the optical depth to lensing with image separations in the range 90–300 mas is several times less than on arcsec scales.

Key words: galaxies: active – galaxies: compact – galaxies: jets – gravitational lensing – radio continuum: galaxies.

1 INTRODUCTION

Systematic searches for gravitational lenses on the arcsec scale have been carried out over the past decade at both optical and radio wavelengths. Among the radio searches are the Jodrell Bank–VLA Astrometric Survey (JVAS – Patnaik et al. 1992; Browne et al. 1998a; Wilkinson et al. 1998) and Cosmic Lens All-Sky Survey (CLASS – Myers 1996) surveys of flat-spectrum sources carried out using the VLA in A configuration; at 8.4 GHz the resolution, ~ 200 mas, is ideal for the initial candidate selection. So far, the JVAS and CLASS surveys have found 13 arcsec-scale lenses of which 12 are new (Browne et al. 1998b list 11 and two more were found recently). Surveys such as these are sensitive to lensing by massive spiral or elliptical galaxies of $\sim 10^{11}$–10^{12} $M_{\odot}$. However, in numerical terms, the galaxy population is dominated by much less massive systems, locally the dwarf galaxies ($\sim 10^{8}$–10^{9} $M_{\odot}$). At cosmological redshifts, results from the *Hubble* Medium Deep Survey (Griffiths et al. 1994) and the *Hubble Deep Field* (Williams et al. 1996) suggest that the majority of objects are compact galaxies, the nature and evolution of which still need to be fully

★Present address: Dep. Matemática, Univ. Madeira, Largo do Colégio, 9000 Funchal, Portugal.

understood (e.g. Lilly, Cowie & Gardner 1991; Glazebrook et al. 1995; Im et al. 1995; Roche et al 1996; Mobasher et al. 1996; Sawicki, Lin & Yee 1997). It is therefore interesting to search for multiple images on an angular scale corresponding to lensing by these compact galaxies. Since the image separation of a gravitational lens is proportional to the square root of the lensing mass, the relevant angular scale is roughly 10 times smaller than that appropriate to individual massive galaxies. It is noteworthy that spiral galaxies can contribute to multiple imaging on scales of < 300 mas (Fukugita et al. 1992) and also that a search in this angular range could place limits on a population of dark compact objects of mass $\sim 10^8$ $M_\odot$ in intergalactic space (Fukugita & Turner 1996).

Our second astrophysical goal was to look for new compact symmetric objects (CSOs) and medium symmetric objects (MSOs). These are symmetric double or triple sources resembling 100 kpc-scale doubles (large symmetric objects – LSOs) but with sizes $\leq$15 kpc. Their 'lobes' are sufficiently compact that self-absorption produces a spectrum which is flatter than $\alpha \sim 0.75$ (defined as $S_\nu \propto \nu^{-\alpha}$), which is typical of LSOs (Fanti et al. 1995). The significance of $\lesssim$1 kpc CSOs and 1–15 kpc MSOs has only recently been recognized (Wilkinson et al. 1994; Readhead et al. 1996a,b; Fanti et al. 1995), largely as a result of the Caltech–Jodrell Bank VLBI surveys (CJ1, Polatidis et al. 1995; Thakkar & et al. 1995; Xu et al. 1995; CJ2, Taylor et al. 1994; Henstock et al. 1995) and MERLIN/VLBI surveys of compact steep-spectrum sources (e.g. Fanti et al. 1995). These surveys have revealed that CSOs and MSOs comprise 5–10 per cent of flux-limited samples of high-luminosity sources. The most plausible evolutionary scenario (Fanti et al. 1995; Readhead et al. 1996a,b) is that CSOs are young (10^3 to 10^4 years) and evolve first into the 10 times larger MSOs and finally into the 100–1000 times larger LSOs. The present search for gravitational lenses should also show up CSOs and MSOs with angular sizes in a previously unexplored range, which may therefore shed new light on the evolution of symmetric radio sources.

The sources on the JVAS and the CLASS samples were selected on the basis of their flat spectra and the great majority are not significantly resolved with the A–array at 8.4 GHz for which the synthesized beam is ~200 mas. However, examination of JVAS and CLASS visibility data allowed us reliably to pick out sources with multiple compact components separated by $\geq$90 mas. By this means we selected 55 lens and CSO/MSO candidates out of a parent sample of 1665 objects; we describe the selection process in detail in Section 2. In order to classify them morphologically, these candidates were observed at higher angular resolution. The initial observations were made with MERLIN at 5 GHz (~50 mas resolution) but if classification was not possible from the MERLIN maps (about 25 per cent of the cases) the candidates were observed with the VLBA at 5 GHz (~2 mas resolution) or, in a few cases, with MERLIN at 22 GHz (~10 mas resolution). These observations and their reduction are described in Section 3 and the resulting maps and morphological classification of the individual sources are presented in Section 4. Further comments on the results, concentrating on CSO/MSOs, are given in Section 5. A more extensive discussion of the implications for gravitational lensing will be presented in Augusto & Wilkinson (1998).

2 THE PARENT SAMPLE AND THE SELECTION OF CANDIDATES

2.1 The starting sample

The two VLA surveys of flat-spectrum sources from which the sample of kpc-scale flat-spectrum radio sources was selected were both made in A configuration at 8.4 GHz and at a resolution of ~200 mas. JVAS covers the northern celestial hemisphere (excluding a $\pm 2\overset{\circ}{.}5$ strip centred on the Galactic plane) and contains ~ 2300 radio sources. At the time of the selection of our candidates, CLASS contained ~ 2400 sources and covered only the declination strip $\delta = 35$–$75°$. The CLASS sources are on average weaker (limiting flux density 25 mJy at 5 GHz) than the JVAS sources (limiting flux density 200 mJy at 5 GHz). From these ~ 4700 sources a smaller parent sample was selected using the following criteria:

(i) $S_{8.4} \geq 100$ mJy;
(ii) $\alpha_{1.4}^{4.85} < 0.5$;
(iii) $|b^{II}| > 10°$.

The reasons for adopting these criteria were: (i) to concentrate on the stronger sources which are easier to map at higher resolution; (ii) to select only sources with bona fide flat spectra, so that the search is less confused by sources with intrinsically more complex structures; the 1.4-GHz flux densities come from White & Becker (1992) and the 4.85-GHz flux densities from Gregory & Condon (1991); (iii) to avoid the Galactic plane, hence facilitating optical follow-up.

From this initial parent sample we immediately had to reject some objects because of large initial position errors in the JVAS and the CLASS observations. As explained in detail in Patnaik et al. (1992), an initial position error can mimic resolution of an unresolved source as a result of bandwidth smearing. All sources with position errors > 30 arcsec were rejected leaving a parent sample of 1665 objects (249 of which were from CLASS).

2.2 The selection of the sample of kpc-scale sources

Our primary goal was to look for high-magnification (flux ratio $\lesssim$ 8:1) gravitational lenses in which the multiple images have separations < 300 mas. It is difficult to recognize lensing effects on diffuse emission with the snapshot mapping techniques we employed and so we looked only for cases where compact structure (a core) is lensed into multiple images. We picked candidates by examining the VLA visibilities of the objects in the parent sample by eye, selecting those which exhibited a $\gtrsim$25 per cent decrease in correlated flux density from the shortest to the longest baselines.

A significant fraction of the sources we picked out from their visibilities have additional extended structure on scales larger than 300 mas visible on the VLA maps. Typically they are core–jets and are included in the sample of candidates because the visibility data show that their brightest components are separated by $\lesssim$300 mas. Note that the systematic search for JVAS lenses with images separated by > 300 mas is a separate programme and the results are being published elsewhere (King et al. 1998).

The maximum baseline of the A array at 8.4 GHz is ~ 1 Mλ and to establish the range of sources to which our visibility selection criterion was sensitive we analysed simulated VLA data produced with the FAKE program in the Caltech VLBI package (Pearson 1991). We measured by eye the decrease in correlated flux in the same manner as for the real JVAS and CLASS data for many different types of model sources. These had a range of separations, component flux density ratios, position angles of components, declinations and hour angles at which the snapshots were taken. We simulated compact doubles (CD), one-sided core–jet sources (with jets of different strengths relative to the core), mini-FR II type sources (i.e. CSO/MSOs) and a four-component system characteristic of a 'quad' gravitational lens system. In Fig. 1 we show a representation of the CD and the 'quad' used in the simulations (e.g. on a scale of

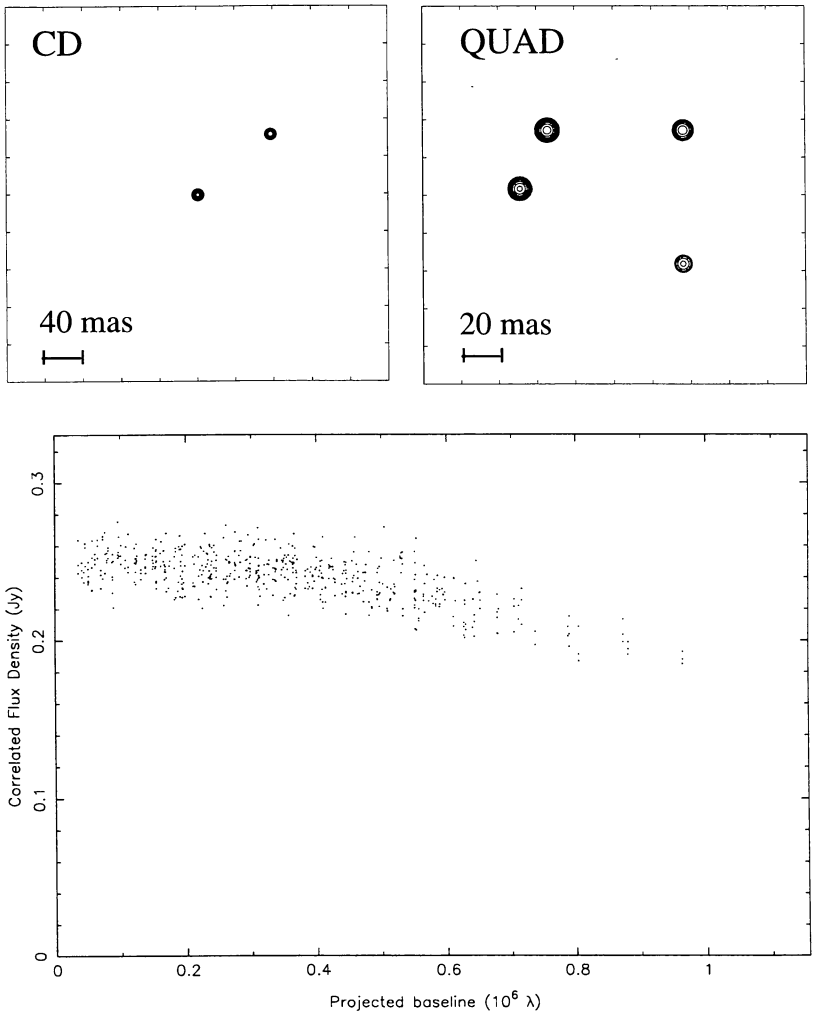

Figure 1. (Top) Two of the source models used in simulating the sensitivity of our visibility selection criterion to a range of source types. The simplest compact double model on the left produces broadly similar results to one-sided core–jet models with compact knots in the jets and to mini-FRII models having additional extended lobe-like structure. On the right is a model 'quad' which is representative of the five such arcsec-scale systems found so far in the JVAS and the CLASS surveys. Visibility data corresponding to observations with the VLA A–array at 8.4 GHz were produced for models with angular sizes in the range 50–300 mas and for a range of component flux densities to determine the observational selection thresholds. The results of these simulations are summarized in Fig. 2. (Bottom) A model visibility plot for a resolved source showing a visually estimated 25 per cent decrease in correlated flux density from the shortest to the longest baselines.

100 mas). In the same figure we also show a simulation of a typical visibility versus baseline plot for a source resolved by ~25 per cent on the longest baselines.

The results of the simulations are summarized in Fig. 2. They were broadly similar for the various models. At a separation of 90 mas, only sources with roughly equal components are selected with high reliability. As the separation increases the flux density ratio detection threshold (R) increases, until at separations larger than 160 mas sources with flux density ratios of $\gtrsim$7:1 are reliably selected. Formally, a ~ 200 mas double with flux density ratio of 7.5:1 would produce a 23.5 per cent decrease of correlated flux on the longest VLA baselines, but in order not to miss any high-magnification lenses we were consistently cautious estimating the reduction in visibility on the longer baselines. The 7:1 flux density ratio line, presented in Fig. 2, corresponds to a 25 per cent decrease of correlated flux from the shortest to the longest baselines. It is important to note that Fig. 2 presents a cautious picture of the angular separation/R parameter space. In fact, our visibility

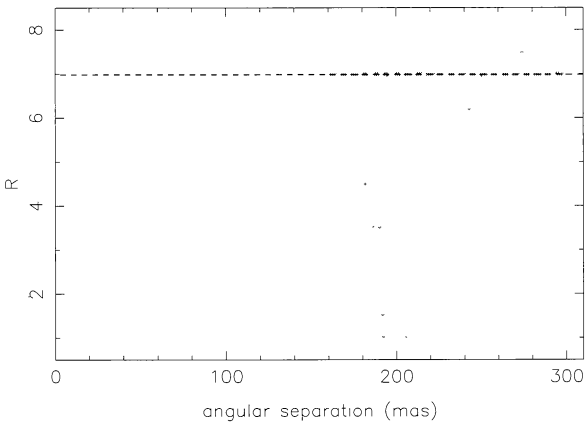

Figure 2. The angular separations of sources having multiple compact components with maximum flux density ratio R, which will be selected from VLA A-array data at 8.4 GHz using the criterion of a ~ 25 per cent decrease in correlated flux density from the shortest to the longest baselines. In the shaded region sources will be picked with near 100 per cent reliability.

Table 1. The 55 flat-spectrum sources with kpc-scale structure: **(1)** IAU object name, 1950.0 equinox; **(2,3)** RA and Dec. from the JVAS/CLASS (2000.0 equinox); **(4)** optical identification on the POSS (Palomar Observatory Sky Survey) plates: G – galaxy; EF – empty field (no objects within 5 arcsec); R-BSO – red-blue stellar object; **(5)** visual magnitude estimated by eye from the POSS plates; **(6)** redshift and reference; **(7)** spectral index between 1.4 and 4.85 GHz with flux densities from White & Becker (1992) and Gregory & Condon (1991), respectively; **(8)** percentage polarization at 8.4 GHz from the JVAS; **(9)** classification of the radio structure from results in this paper except for the sources with NM or Q in column (10); **(10)** candidates ruled out with high-resolution maps available in the references given: Q, object mapped for quality control purposes alone: NM, object not mapped by us. References for columns (6) and (10): 1: Stickel & K uhr (1996a); 2: King (1995); 3: Polatidis et al. (1995); 4: Burbidge & Crowne (1979); 5: Puchnarewicz et al. (1992); 6: Xu et al. (1995); 7: Unger et al. (1984); 8: Wrobel & Simon (1986); 9: Henstock et al. (1995); 10: Allington-Smith et al. (1988); 11: Unger et al. (1986); 12: Sargent (1973); 13: Wills & Wills (1976); 14: Sykes (1997); 15: Le Borgne et al. (1991); 16: Baldwin et al. (1973); 17: Vermeulen et al. (1996); 18: March a et al. (1996); 19: Browne et al. (1993); 20: Patnaik et al. (1993); 21: Hook et al. (1996); 22: Henstock et al. (1997); 23: Stickel et al. (1996).

Source	J2000.0 positions		optical identification			$\alpha_{1.4}^{4.85}$	% pol	Radio morphology	Notes
	RA	δ	id	m	z				
(1)	(2)	(3)	(4)	(5)	(6)	(7)	(8)	(9)	(10)
B0046+316	00 48 47.144	31 57 25.09	G	15.0	0.015 [11]	0.05	1.1	bright-core CSO	Q [7]
B0112+518	01 15 56.874	52 09 13.03	EF	>21		0.37	3.9	faint-core CSO/MSO?	
B0116+319	01 19 34.999	32 10 50.01	G	16.0	0.0592 [12]	0.47	0.3	faint-core CSO	Q [8]
B0127+145	01 29 55.348	14 46 47.84	BSO	19		0.22	7.9	core+90° bent jet	
B0205+722	02 09 51.792	72 29 26.67	G	18.0	0.895 [17]	0.33	3.2	bright-core MSO	
B0218+357	02 21 05.470	35 56 13.72	RSO	20.2	0.685[1] [19]	−0.01	5.8	335 mas lens	NM [20]
B0225+187	02 27 53.335	19 01 14.08	EF	>21		0.48	2.8	faint-core CSO/MSO?	
B0233+434	02 37 01.215	43 42 04.20	EF	>21		0.45		faint-core CSO	
B0345+085	03 48 10.418	08 42 08.87	EF	>21		0.21	0.7	core+90° bent jet	
B0351+390	03 55 16.591	39 09 09.82	BSO	19.6		−0.14	4.4	core–jet	
B0352+825	04 02 12.674	82 41 35.10	G	15.5		0.28[2]	0.6	bright-core CSO	
B0418+148	04 20 51.086	14 59 15.63	EF	>21		0.32	1.5	core+90° bent jet	
B0429+174	04 31 57.380	17 31 35.79	EF	>21		0.37	4.5	core+90° bent jet	
B0529+013	05 32 08.776	01 20 06.33	RSO	20		0.42	6.8	core–jet	
B0638+357	06 41 35.854	35 39 57.62	EF	>21		0.44	1.6	bright-core MSO	
B0732+237	07 35 59.928	23 41 02.75	EF	>21		0.37	0.6	faint-core CSO/MSO	
B0817+710	08 22 16.765	70 53 07.98	EF	>21		0.37	0.0	faint-core MSO?	
B0819+082	08 22 33.154	08 04 53.52	RSO	19.3		0.30[b]	1.4	faint-core MSO?	
B0821+394	08 24 55.484	39 16 41.90	BSO	18.0	1.216 [13]	0.07	1.6	core–jet (compact knot)	NM [6]
B0824+355	08 27 38.589	35 25 05.08	RSO	19.6	2.249 [10]	0.12	2.5	LSO/bright-core MSO ?	Q [9]
B0831+557	08 34 54.903	55 34 21.09	G	17.5	0.242 [4]	0.07	0.0	LSO	NM [3]
B0905+420	09 08 35.862	41 50 46.20	BSO	19.5		0.16	1.8	core+90° bent jet	
B0916+718	09 21 23.94	71 36 12.42	BSO	18.5	0.594 [1]	0.06	0.8	core–jet	NM [2]
B1003+174	10 06 31.765	17 13 17.10	BSO	20.5		0.31	1.4	core+> 90° bent jet	
B1010+287	10 13 03.000	28 29 10.93	EF	>21		0.49	0.6	faint-core CSO?	
B1011+496	10 15 04.136	49 26 00.69	BSO	16.8	0.2 [5]	0.23	2.5	core–jet	
B1058+245	11 01 23.514	24 14 29.52	EF	>21		0.47	11.0	faint-core MSO?	
B1143+446	11 45 38.519	44 20 21.92	RSO	20.0	0.30 [21]	0.23	2.2	core+90° bent jet	
B1150+095	11 53 12.550	09 14 02.31	BSO	18.0	0.698 [13]	0.31	1.6	core+90° bent jet	
B1211+334	12 14 04.113	33 09 45.56	BSO	17.2	1.598 [13]	0.49	2.3	core–jet (compact knot)?	
B1212+177	12 15 14.722	17 30 02.25	RSO	20		0.24	0.0	faint-core CSO/MSO	
B1233+539	12 35 48.252	53 40 04.84	BSO	19		0.48		faint-core CSO/MSO?	
B1241+735	12 43 11.216	73 15 59.26	G	17.0	0.075 [18]	0.33	0.0	core–jet	
B1317+199	13 19 52.074	19 41 35.48	EF	>21		0.45	2.7	core+90° bent jet	
B1342+341	13 44 37.102	33 55 46.19	BSO	19.5		0.43	4.1	core+> 90° bent jet	
B1504+105	15 07 21.882	10 18 44.99	—	16		0.39	0.0	faint-core CSO/MSO	
B1628+216	16 30 11.236	21 31 34.38	—	—		0.16	1.3	bright-core MSO	
B1638+124	16 40 47.938	12 20 02.11	EF	>21	1.152 [23]	0.38	0.2	core–jet	
B1642+054	16 44 56.083	05 18 37.06	EF	>21		0.42	0.7	core–jet	
B1722+562	17 22 58.007	56 11 22.30	BSO	19.8		0.41		core–jet	
B1744+260	17 46 48.283	26 03 20.35	G	17.0	0.147 [18]	0.31	1.6	core–jet	
B1801+036	18 03 56.283	03 41 07.58	G	17		0.36	0.9	bright-core MSO	
B1812+412	18 14 22.708	41 13 05.61	BSO	20.0	1.564 [22]	0.15	1.8	core+180° bent jet	
B1857+630	18 57 29.200	63 05 30.04	BSO	19.5		0.38		core–jet	
B1928+681	19 28 20.550	68 14 59.25	BSO	20.5		0.41	4.1	bright-core CSO/MSO	
B1947+677	19 47 42.579	67 57 54.57	EF	>21		0.11		bright-core MSO	NM [14]
B2101+664	21 02 36.631	66 36 34.22	RSO	18		0.33[3]		core–jet	
B2112+312	21 14 50.461	31 30 21.18	EF	>21		0.44	0.9	core+bending jet	
B2150+124	21 53 04.659	12 41 05.21	BSO	19.5		0.38	3.5	core+> 90° bent jet	
B2151+174	21 53 36.827	17 41 43.73	G	17.5	0.231[4] [15]	0.13	0.0	bright-core CSO	

Table 1 – *continued*

Source	J2000.0 positions		optical identification			$\alpha_{1.4}^{4.85}$	% pol	Radio morphology	Notes
	RA	δ	id	m	z				
(1)	(2)	(3)	(4)	(5)	(6)	(7)	(8)	(9)	(10)
B2201+044	22 04 16.934	04 40 06.97	G	15.5	0.028 [13]	0.07		core–jet	
B2205+389	22 07 46.072	39 13 50.35	EF	>21		0.33	0.0	core–jet	
B2210+085	22 13 21.737	08 47 29.95	RSO	17.8		0.07	2.9	core–jet	
B2247+140	22 50 25.343	14 19 52.04	RSO	17.5	0.237 [16]	0.48	2.3	core+> 90° bent jet	
B2345+113	23 47 36.406	11 35 17.89	G	19		0.36	1.3	bright-core CSO/MSO?	

[a]Lawrence (1996) give $z = 0.96$ for the lensed object.
[b]1.4-GHz flux densities from the NVSS (Condon et al. 1998).
[c]Calculated from our MERLIN *L*-band observations at 1.66 GHz.
[d]Assuming membership of the cluster Abell 2390.

criterion would select equal doubles down to 50 mas separation about half the time – depending on the hour angle of the snapshot, the source declination and position angle of the source elongation. About 88 per cent of the time we select equal doubles with 60 mas separation and 97 per cent of the time we select 75 mas equal doubles. In subsequent analysis of the lensing statistics we will make no claims about such small separation sources but will restrict ourselves to the sources with separations which can be detected with high reliability.

2.3 The candidates

The percentage of radio sources we selected as lens or CSO/MSO candidates from the parent sample is ~3 per cent. They total 55 (of which 49 are from JVAS and six are from CLASS) and are listed in Table 1. Their radio spectra are presented in Appendix A. The majority of the sources in the kpc-scale sample have power-law spectra down to ~300 MHz; the absence of synchrotron self-absorption therefore implies that all should have structure on $\gtrsim$20 mas scales. There are no GHz peaked spectrum sources (GPS) among the sample, indicating that none of them is dominated solely by milliarcsec-sized subcomponents.

Eight of the candidates had been previously observed by others at high resolution and their morphology is known. We followed up three of these as quality control for the MERLIN snapshot observations (marked 'Q' in Table 1). The remaining five, which were not mapped by us, are denoted as 'NM' in Table 1.

2.4 Establishing the morphological classification

In order to classify these flat-spectrum sources with kpc-scale structure, we adopted a systematic strategy of mapping them at increasingly higher angular resolution. We considered that the jump to the mas resolution afforded by VLBI was too large to make in one step, in view of the danger of missing weak compact components in maps extending over hundreds of resolution elements. We therefore adopted the principle of first observing all the 50 sources (those not designated 'NM' in Table 1) with MERLIN at 5 GHz which provides a resolution of 50 mas.

At the MERLIN resolution, lensed cores would look like unresolved doubles or quads while CSO/MSOs would be doubles or triples with marginally resolved or unresolved components. Any candidate lenses or CSO/MSOs were then observed with the VLBA at 5 GHz which provides a resolution of ~2 mas. At this resolution only multiply imaged cores would be expected to remain unresolved or marginally resolved. CSO/MSOs might have a detectable central compact core but the outer components are expected to be resolved in the VLBA map.

The decision as to which sources to observe with the VLBA is particularly important in the case of lens candidates. The criterion we used for identifying lens candidates was based on the fact that the true surface brightness of gravitationally lensed images of a given object must be the same. Weaker secondary images must be demagnified and hence smaller than the primary image. Thus if a weaker component in the MERLIN map was larger than the strongest component, so that its surface brightness was three or more times smaller, the source was ruled out as a lens candidate and was not observed with the VLBA.

3 OBSERVATIONS AND DATA REDUCTION

3.1 The MERLIN 5-GHz observations

To follow up the 50 candidates we employed a snapshot technique which enabled us to complete the observations within five days of observing time. Since this was the first major programme of snapshot observations with MERLIN, we carried out a series of simulations (using FAKE and DIFMAP in the Caltech VLBI package – Pearson 1991; Shepherd, Pearson & Taylor 1994) to determine how well such snapshot data can be used to reproduce the structure of radio sources with angular extent $\lesssim$ 1 arcsec. Full details of these simulations are given by Augusto (1996). In Fig. 3 we show the results of one representative simulation only. Using the same types of models as for determining Fig. 2, we showed that the six telescopes of MERLIN give adequate *u*,*v* coverage to allow morphological classification of compact sources from four snapshots of 15 min each. A further confirmation of our ability to classify compact radio sources reliably with MERLIN snapshots comes from comparing published maps with our own results for the three 'quality control' sources in Table 1 (designated 'Q').

The phase-referencing technique was used to calibrate the interferometer phase and the observational procedure for each snapshot was as follows: i) observe the phase-reference source for 2 min; ii) observe the target for 16 min; iii) observe the phase-reference source for 2 min. Four such snapshots, each 2–3 h apart, were taken for all the candidates. The observations totalled five days spread over several periods in 1995: April 5–6, June 2–5, June 14–15 and July 8. In this final session the Defford telescope was not working properly and all the data from this telescope had to be deleted; nevertheless useful results were still obtained. For

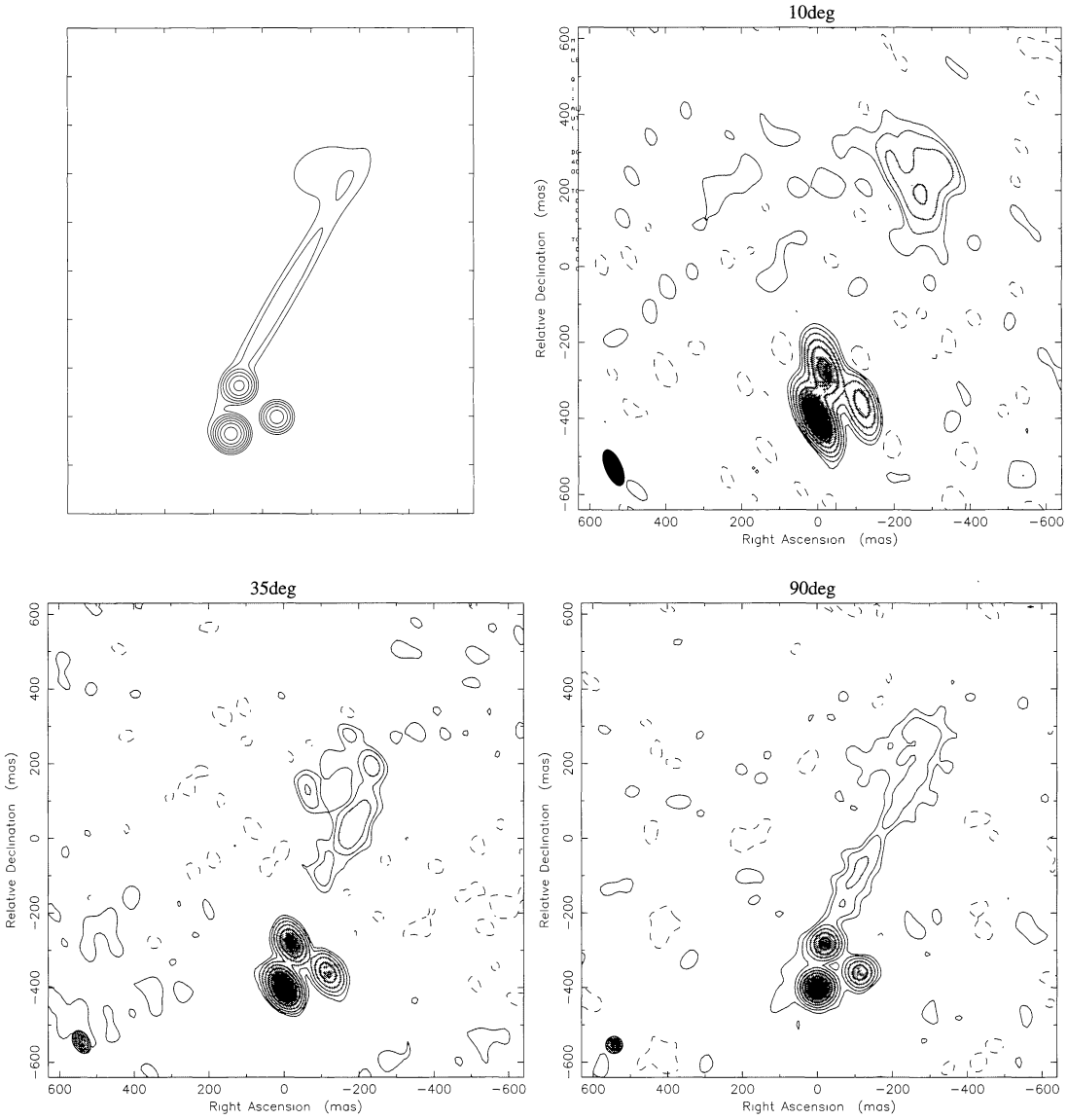

Figure 3. A representative of the many tests we used to assess the suitability of MERLIN 1-h snapshots for the morphological classification of compact radio sources. At the top left is the model and at the top right the map made from simulated data at $\delta = 10°$; below are the corresponding maps at $\delta = 35°$ and at $\delta = 90°$.

amplitude calibration we used the point sources B0552+398, B2134+004 and OQ208. The absolute flux density calibration was established by observation of 3C286 and taking its flux density to be 7.30 Jy as given by Baars et al. (1977). The final correlated flux densities should be accurate to better than 5 per cent.

After initial calibration and editing using the MERLIN 'd' programs, the MERLIN AIPS 'pipeline' was used to produce an initial map of each source automatically. The FITS file of the corrected data was then read into DIFMAP for final mapping. In making these naturally weighted maps we were aided by having the VLA A array map and the pipeline maps as a guide to the structure of each source. The MERLIN 5-GHz maps are presented in Fig. 4 and the map parameters are listed in Table 2. In order to make quantitative judgements about component surface brightness we fitted Gaussian models to the MERLIN data on all sources. In Table 3 we present the best-fitting models for each of the MERLIN 5-GHz maps. Based on our inspection of the MERLIN 5-GHz maps, 14 potential lens or CSO/MSO candidates were selected to be followed up at higher resolution.

3.2 The VLBA 5-GHz follow-up

We had two VLBA observing sessions, on 1995 November 12 and 1996 July 25 (which included one VLA antenna). We used four to six 6.5-min 'snapshots' per source, without phase-referencing as the sources were strong enough for self-calibration. Given our knowledge of the source structure from the MERLIN map, these snapshots provided enough information for classification, even though the sources are quite large (> 50 mas) when compared with the ~2 mas beam appropriate to the naturally weighted VLBA data. We used the standard AIPS analysis techniques to fringe fit and calibrate the data which were then read into DIFMAP for mapping.

Since we were able to classify three sources (see next subsection) from MERLIN 22-GHz observations undertaken between the two VLBA runs, the total number of lens candidates was reduced to 11.

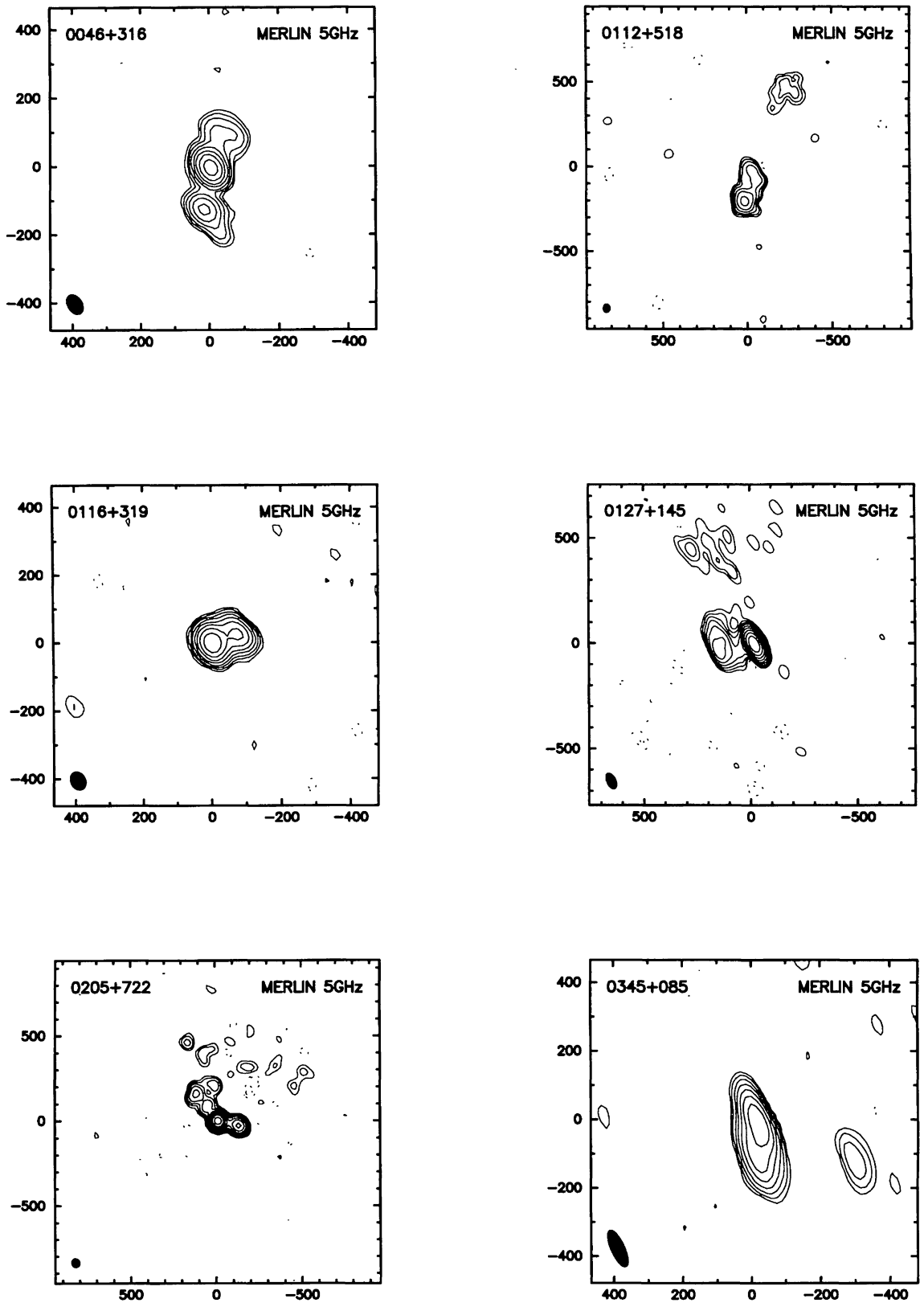

Figure 4. MERLIN 5-GHz maps of 50 sources with kpc-scale structure, together with the MERLIN 22-GHz or VLBA 5-GHz snapshot maps for the 14 candidates that were followed up. The MERLIN 22-GHz maps of B0723+237 and B1211+334 are also presented as we used the corresponding VLBA 5-GHz maps as quality controls for the MERLIN 22- GHz snapshot observations. All the maps are naturally weighted; the FWHM contour of the Gaussian beam is given in the lower left-hand corner and is listed in Tables 2, 4 and 6, along with the peak brightness and lowest contour level drawn at 3σ. Contours are logarithmic at -6σ, -3σ, 3σ, 6σ, etc.; negative contours are shown as dashed lines.

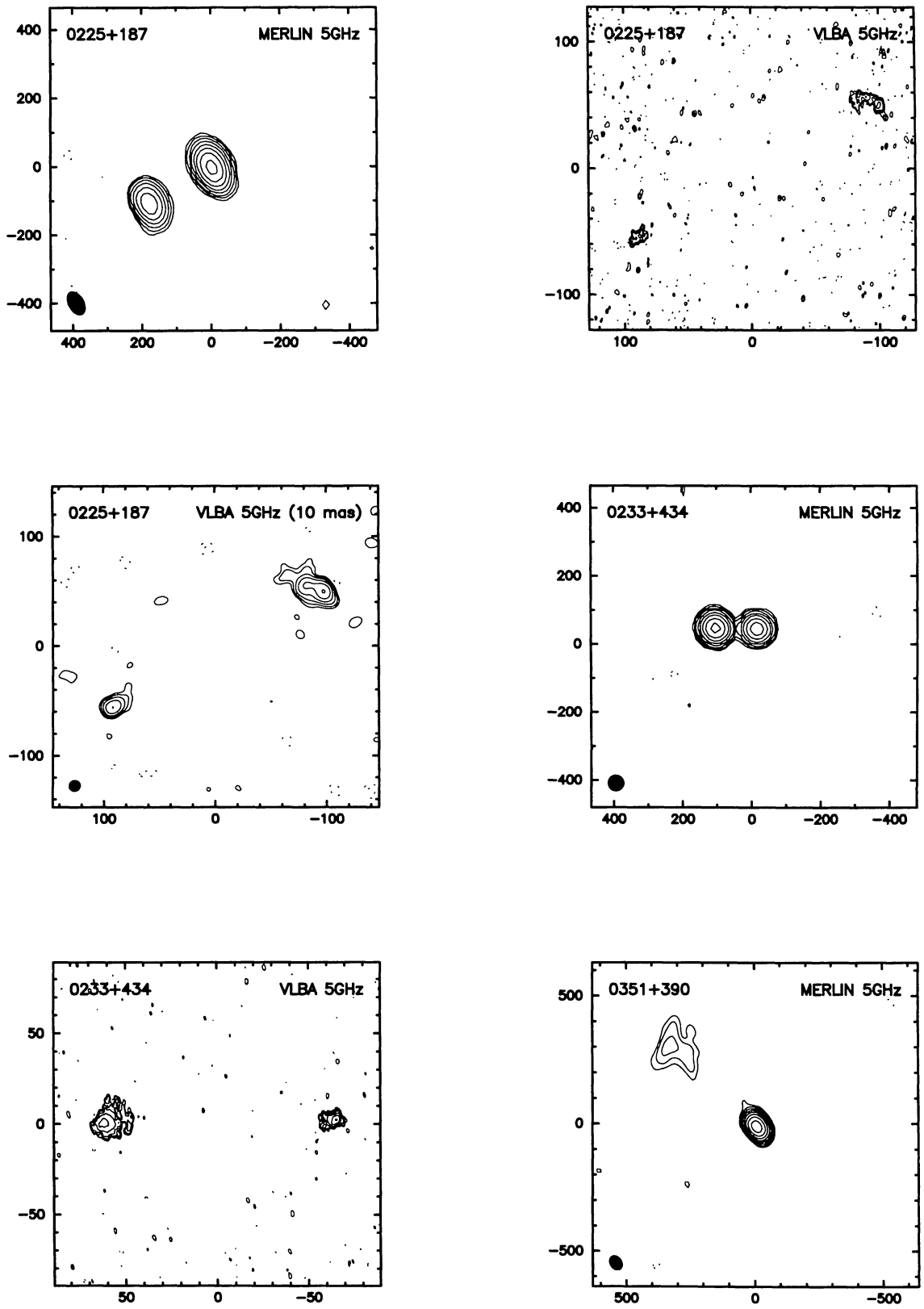

Figure 4 – *continued*

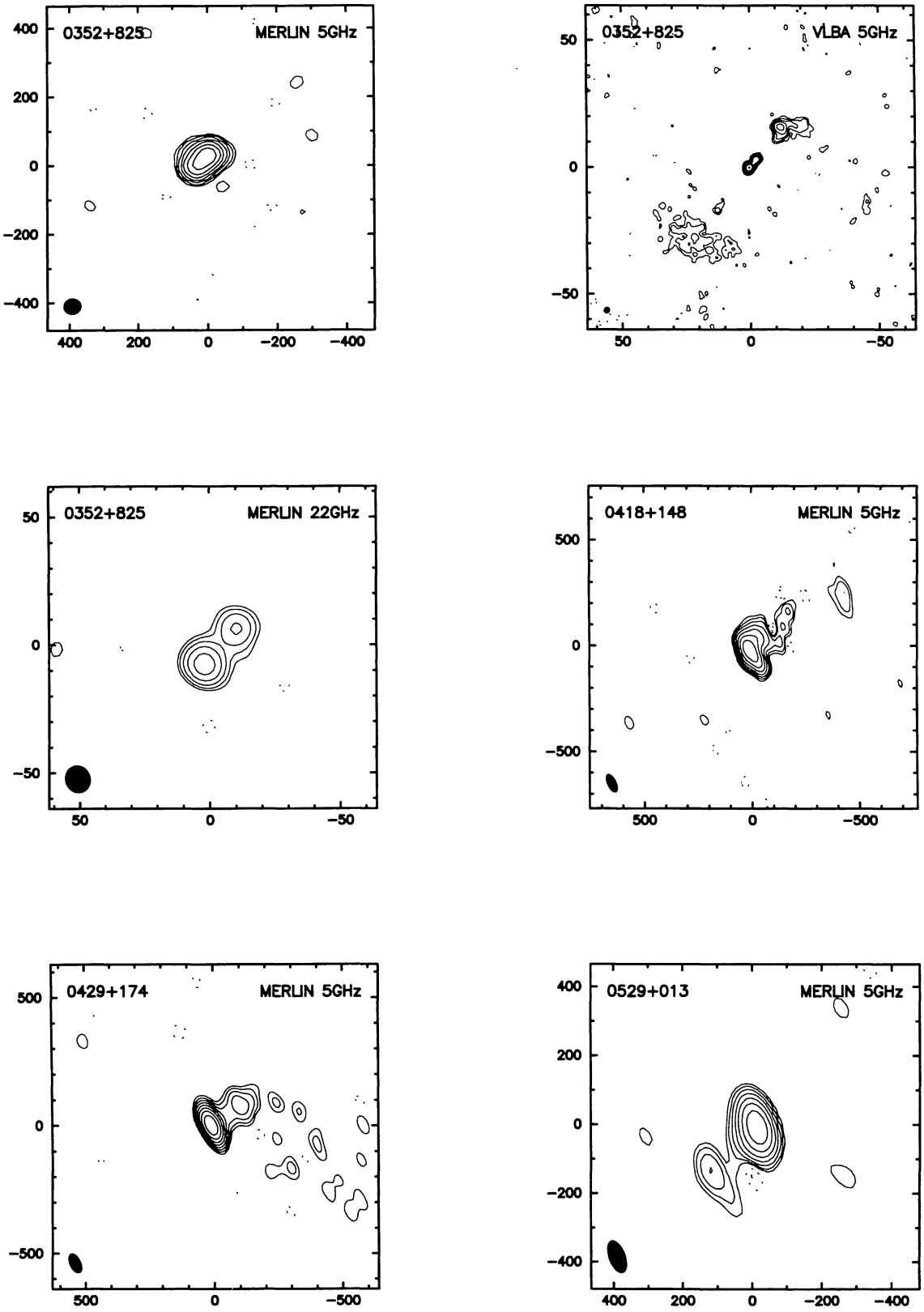

Figure 4 – *continued*

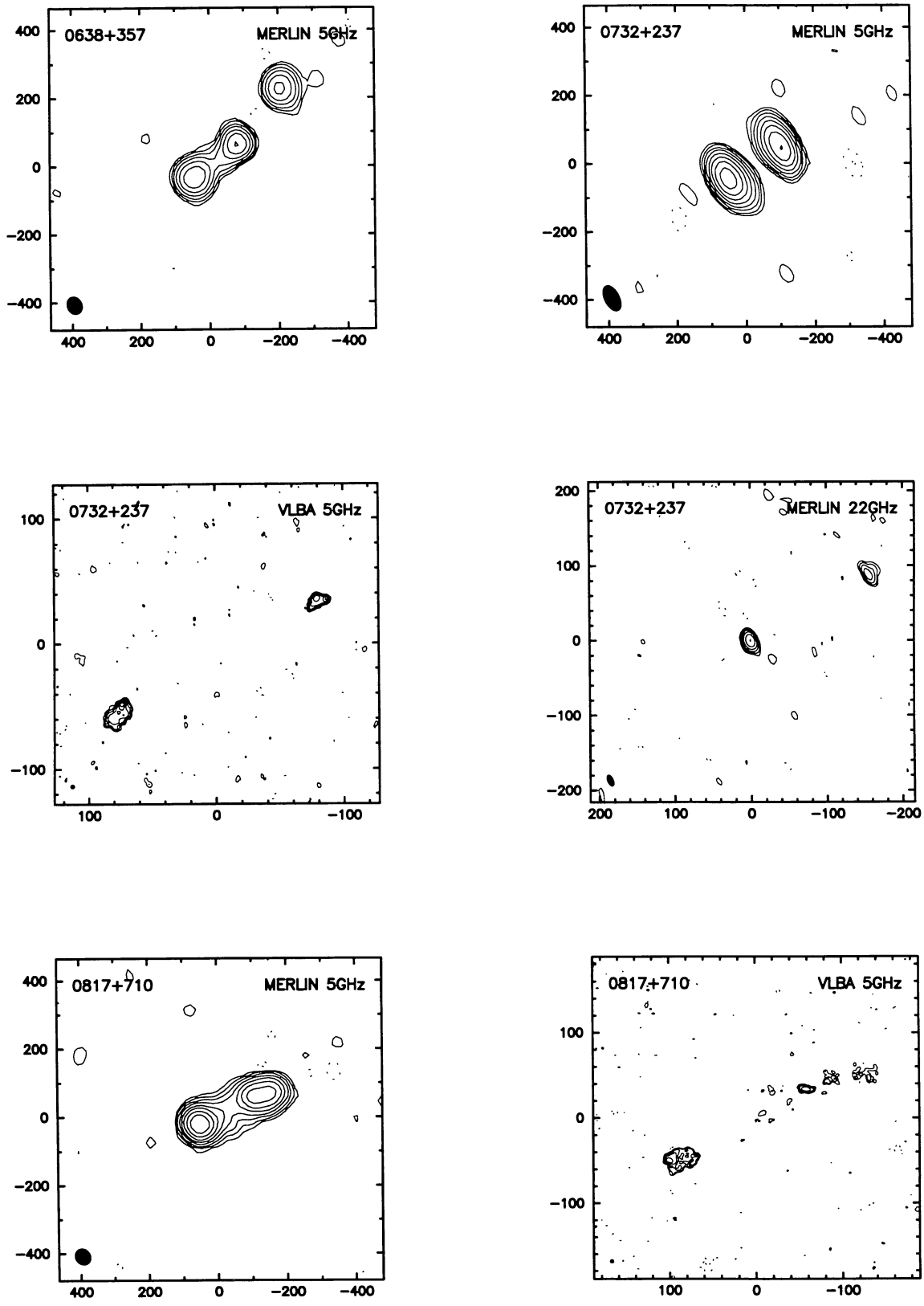

Figure 4 – *continued*

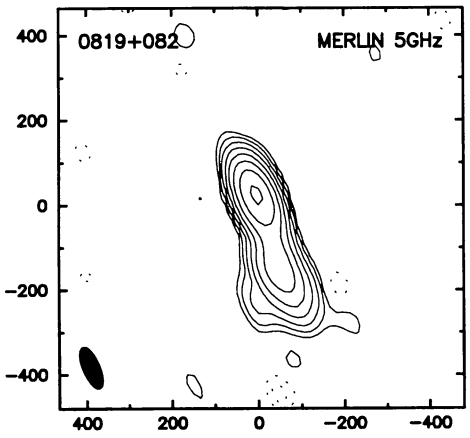

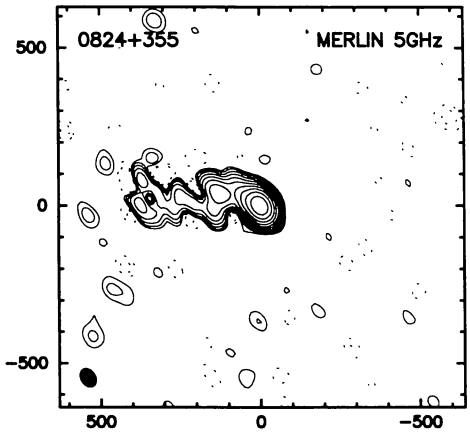

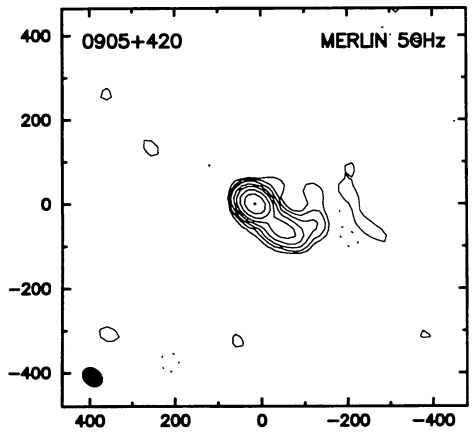

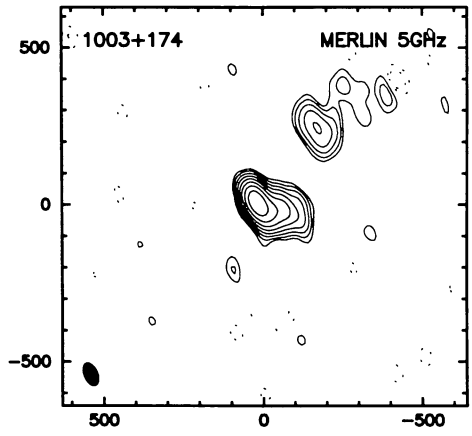

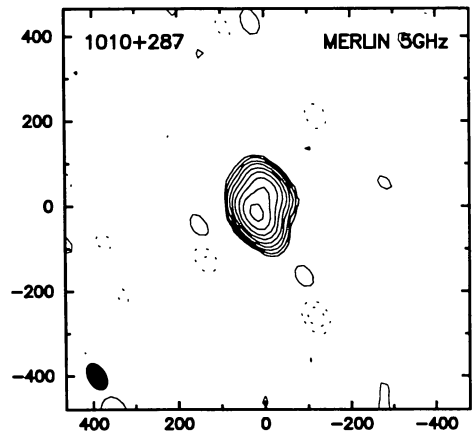

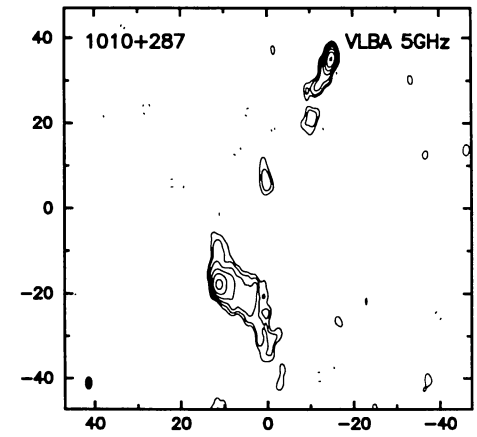

Figure 4 – *continued*

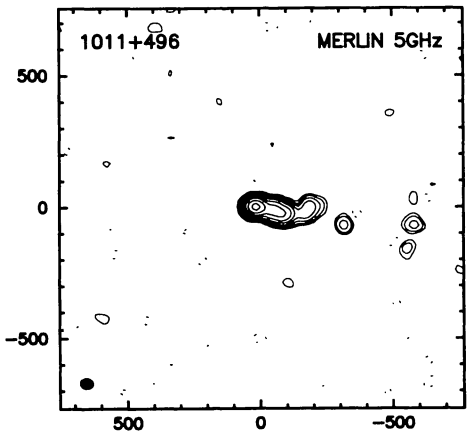

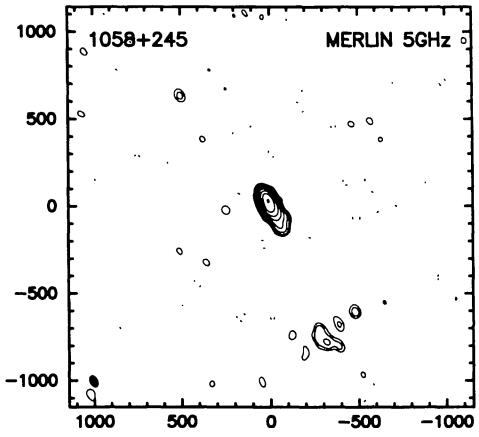

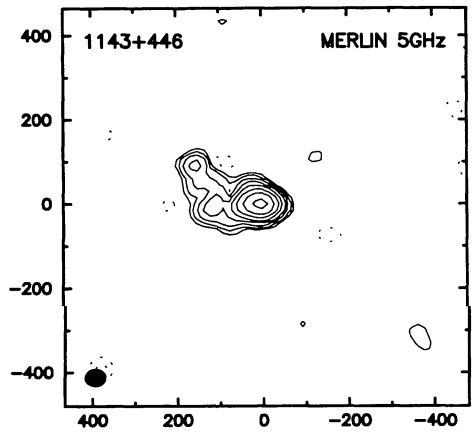

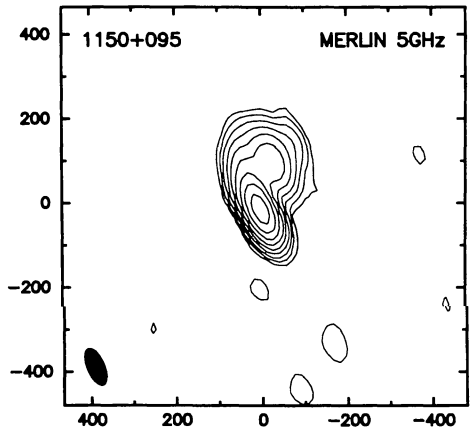

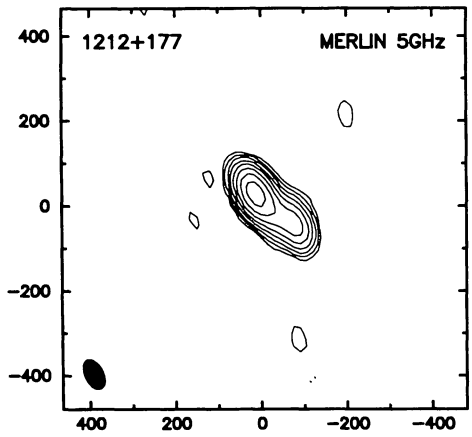

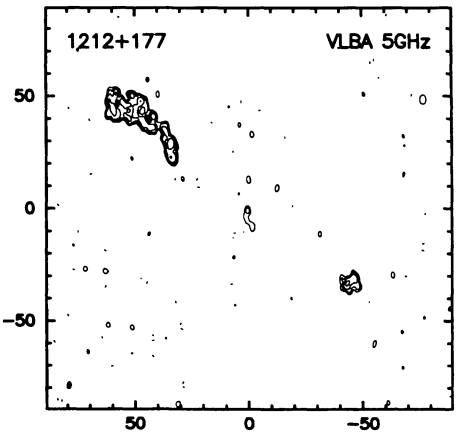

Figure 4 – *continued*

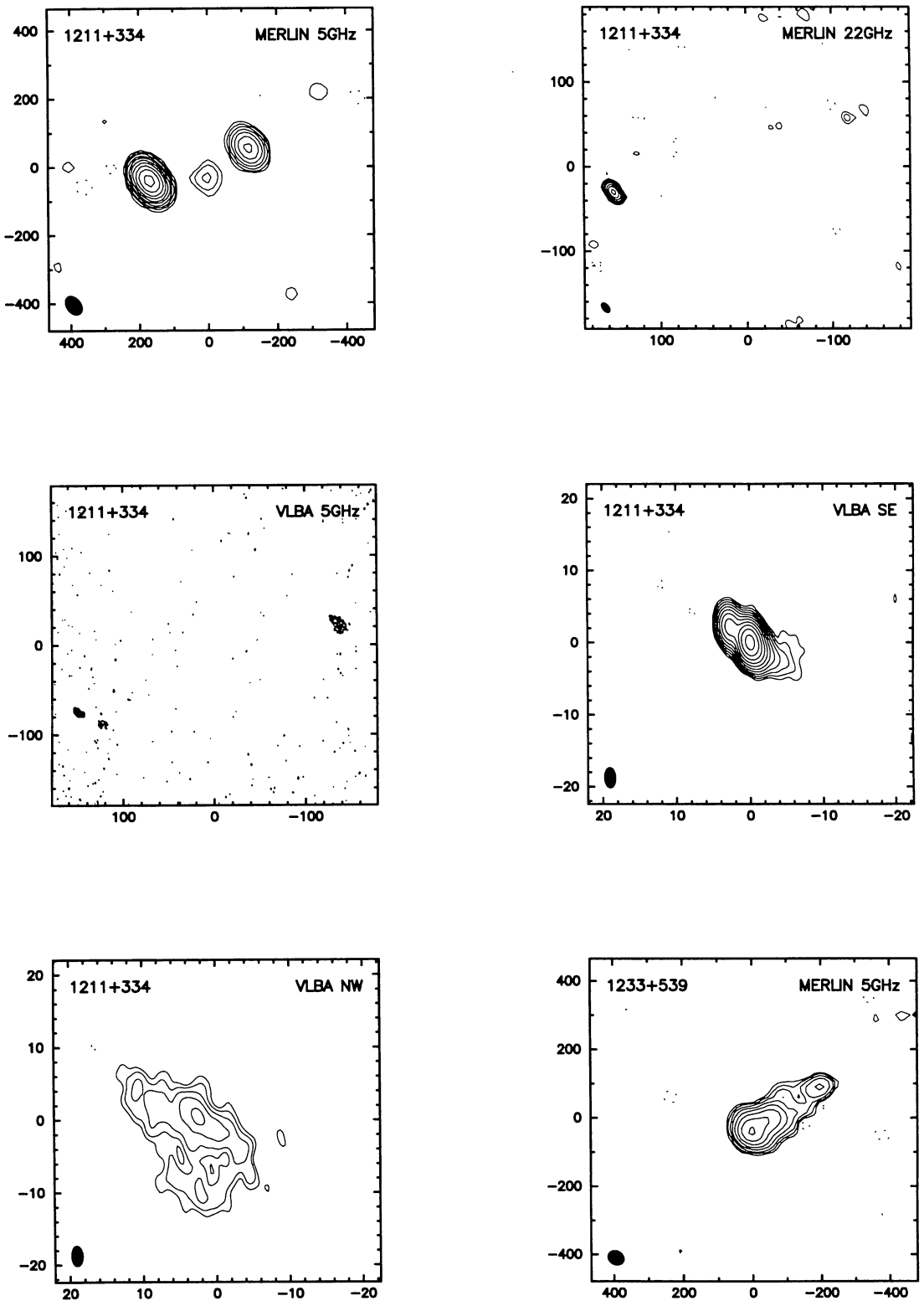

Figure 4 – *continued*

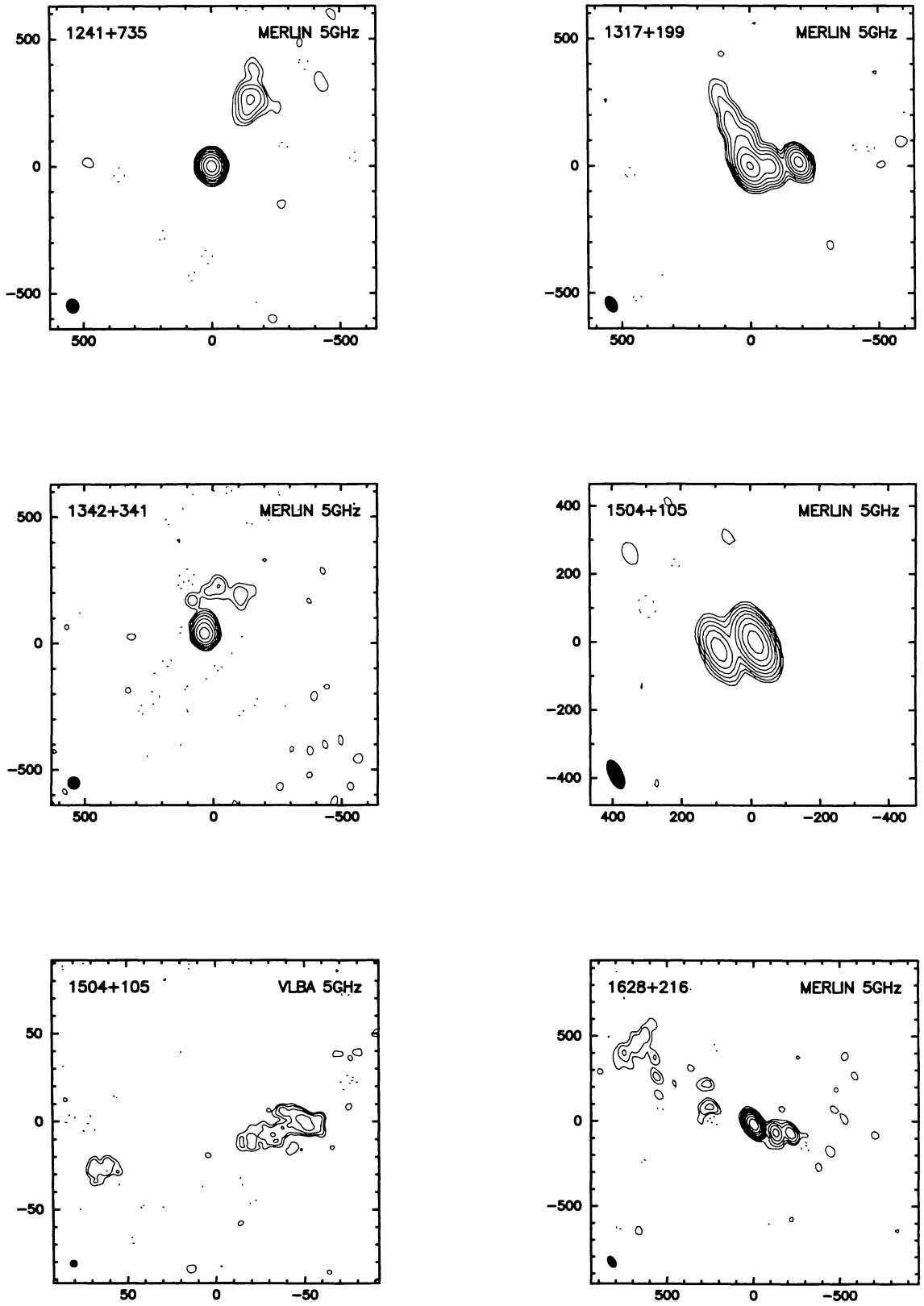

Figure 4 – *continued*

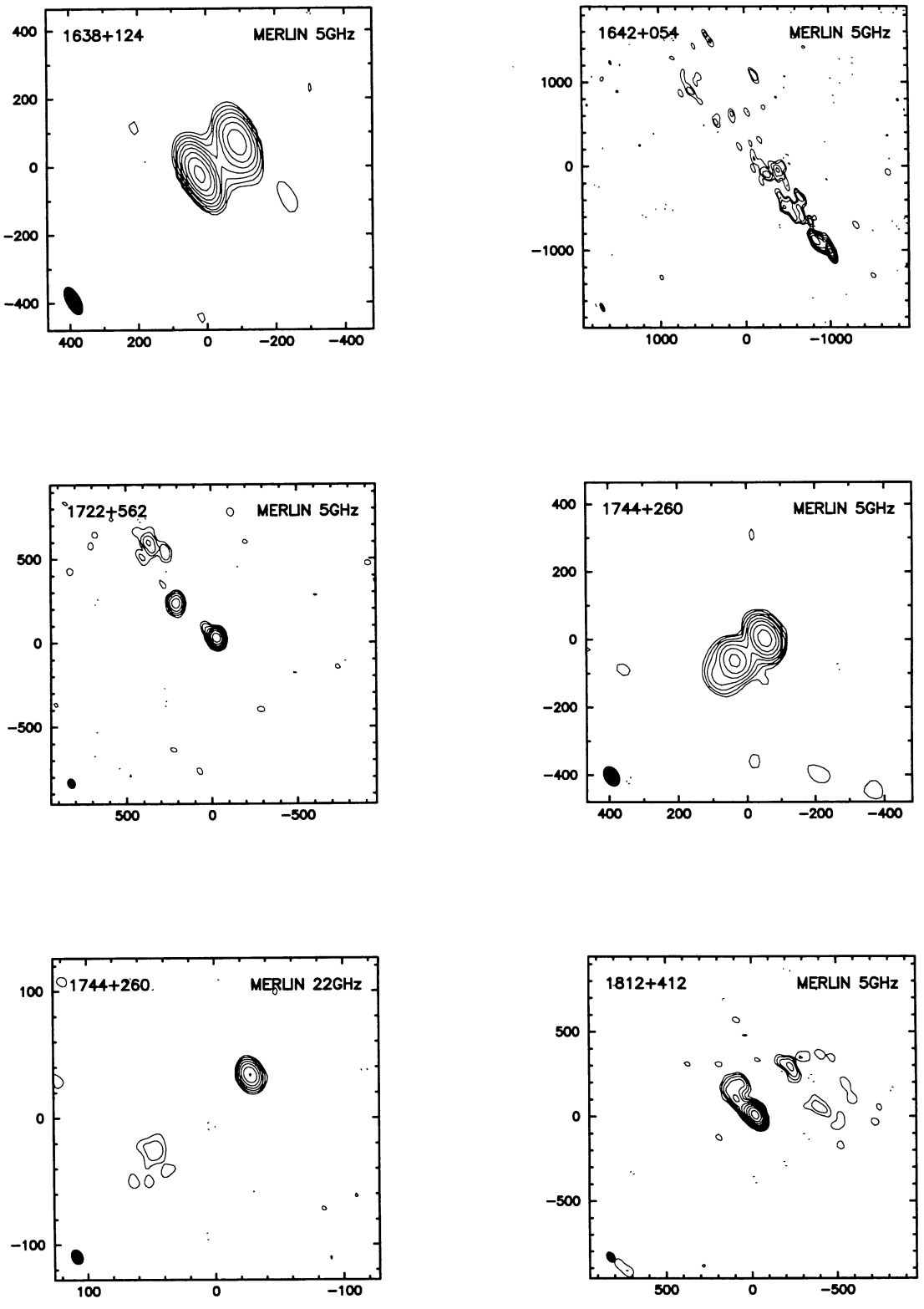

Figure 4 – *continued*

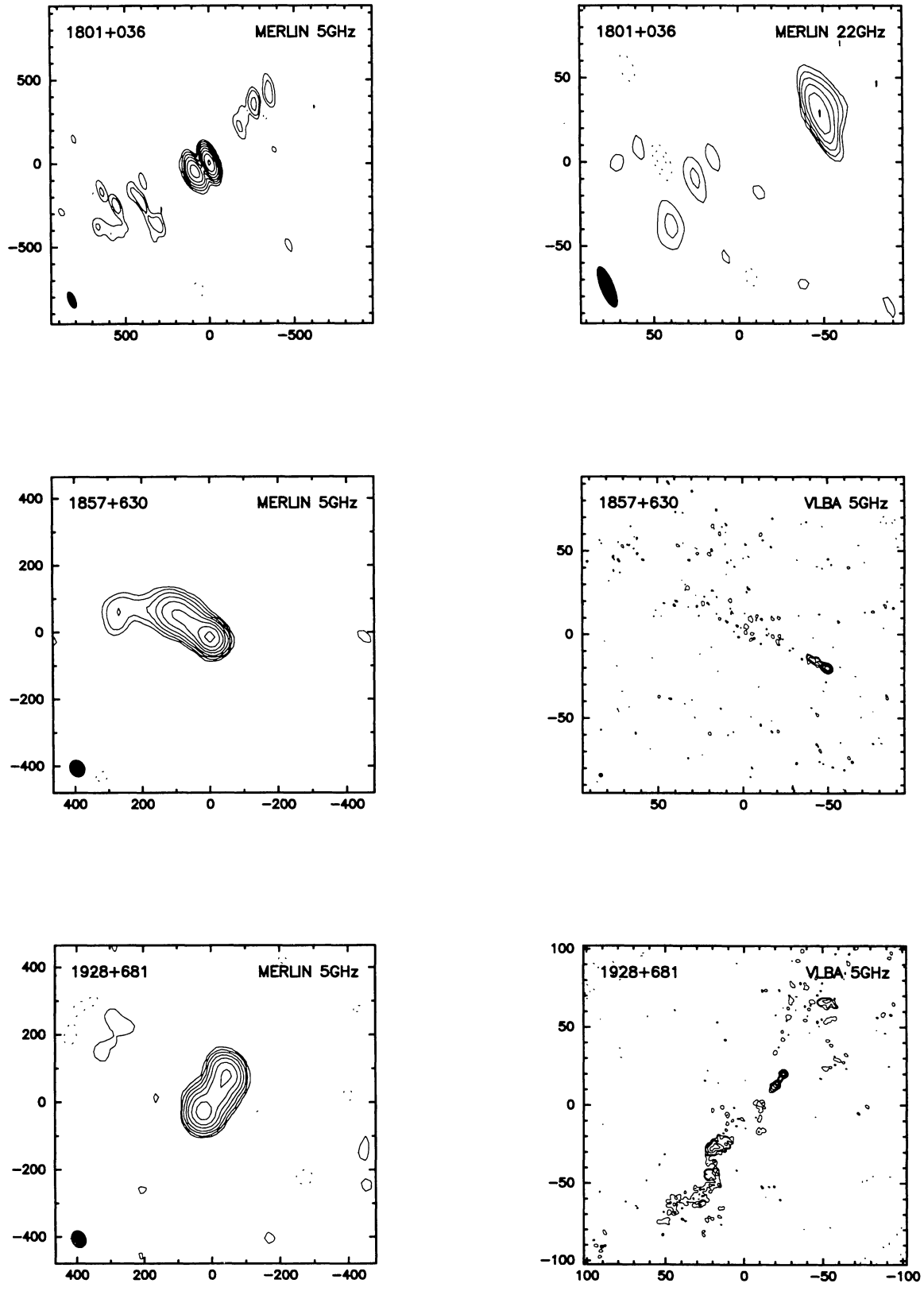

Figure 4 – *continued*

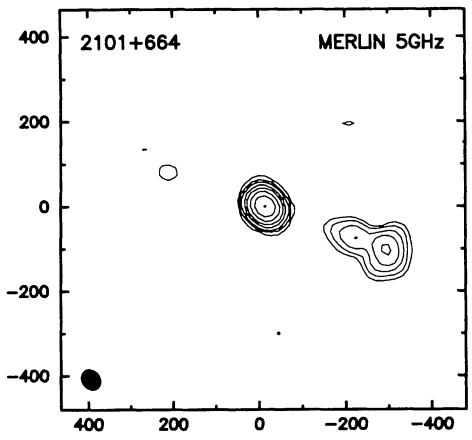

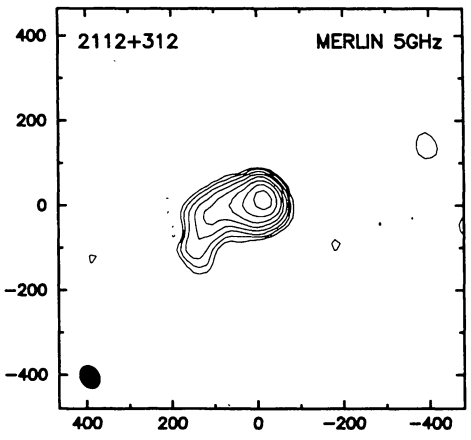

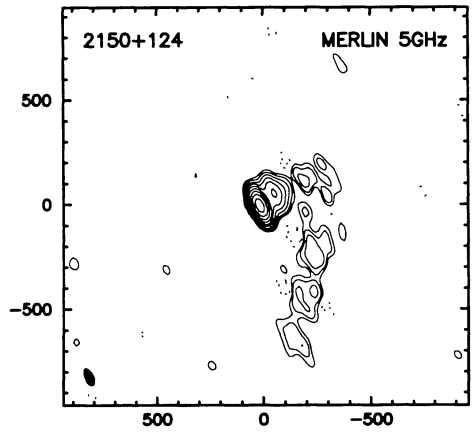

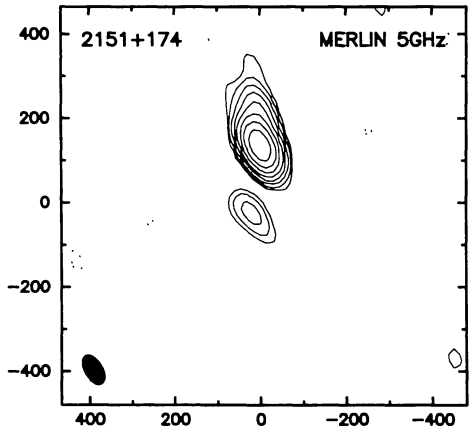

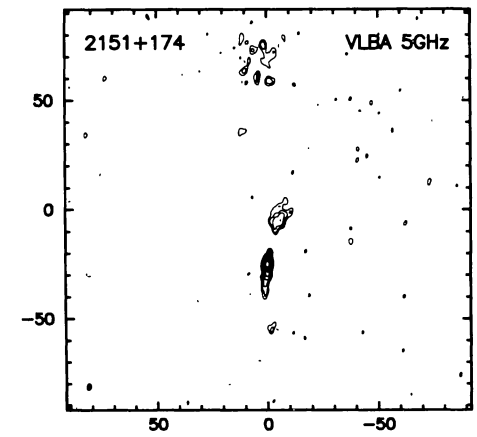

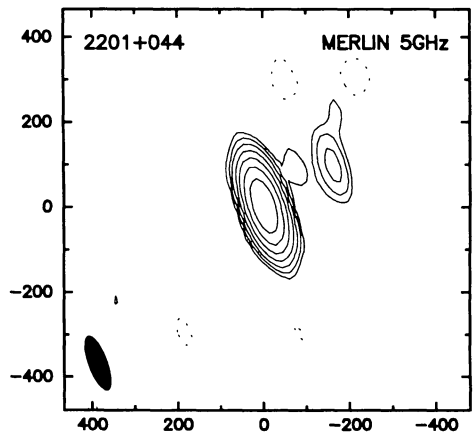

Figure 4 – *continued*

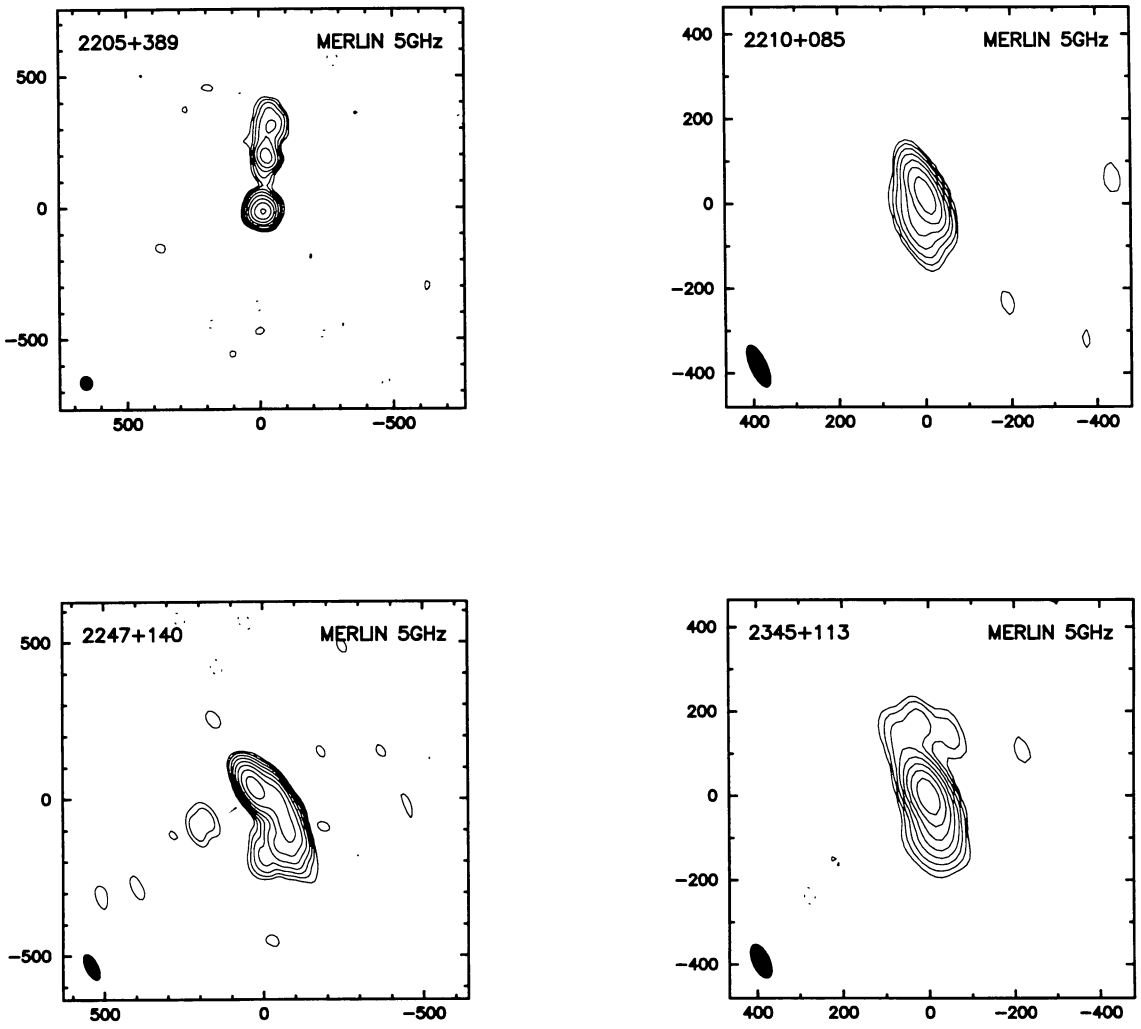

Figure 4 – *continued*

We present 12 maps, however, as although B0352+825 was ruled out from the 22-GHz observations its structure was interesting enough to justify reobservation with the VLBA. The VLBA map parameters are presented in Table 4 and the maps are shown in Fig. 4.

3.3 The MERLIN 22-GHz follow-up

As a complement to the VLBA follow-up we mapped some candidates with MERLIN at 22 GHz. We observed nine sources not observed in the first session of VLBA observations together with two quality control sources (B0732+237 and B1211+334, observed in the first VLBA session) to test the reliability of the 22-GHz maps. These MERLIN observations were much more difficult than those at 5 GHz, not only because the sensitivity at 22 GHz is roughly an order of magnitude worse than at 5 GHz but also because the amplitude and phase stability is highly weather-dependent. It is crucial, therefore, to have the phase calibrator not more than a few degrees away from the target source and to switch very quickly from the target to the phase calibrator and back. Each 91-min snapshot consisted of 14 cycles of 1.5 min on the phase calibrator, 3.5 min on the target and 1.5 min on phase calibrator. Four such snapshots were taken for each target, each separated by about three hours.

The observations were taken in the period 1996 May 10–13 between the two sets of VLBA observations. We used the five MERLIN telescopes which operate at 22 GHz (Cambridge, Knockin, Darnhall, MkII and Tabley) which together provide a resolution of $\sim$ 10 mas. The point-source calibrators used were 3C273 and 3C84, with flux densities, at the epoch of observations, respectively 30.6 and 19.0 Jy (from the monitoring programme at Metsahovi in Finland, H.Teršranta, personal communication; the estimated uncertainty in these flux densities is $\sim$3 per cent).

The maps were produced using the same strategy as that used for the 5-GHz analysis. In view of the difficulty of phase referencing at 22 GHz we often had to rely on self-calibration to correct the visibility phases. For self-calibration to work well, however, the correlated flux density needs to exceed $\sim 2\sigma$ per coherent integration on all baselines at all times. The rms noise (σ) on an individual baseline was typically 25 mJy in a coherent integration time of 1 min. The integrated flux density of most of the sources we observed is only a few σ, hence of the nine sources observed six were too weak to map reliably. However the comparison of the 22-GHz and VLBA maps of the two quality control sources (B0732+237 and B1211+334) shows that as long as a source is strong enough, the MERLIN 22-GHz observations are adequate to test for multiple

Table 2. The parameters for the MERLIN 5-GHz maps.

source B1950.0	beam (mas)	P.A. (°)	map peak (mJy beam^{-1})	1st contour (3σ) (%)
0046+316[a]	63×42	+31	149	0.5
0112+518	52×41	−2	26	2.5
0116+319[a]	57×43	+28	837	0.4
0127+145	81×41	+25	338	0.2
0205+722	54×48	+16	267	0.25
0225+187	73×44	+30	93	0.6
0233+434	47×45	+27	101	0.6
0345+085	117×39	+23	61	0.8
0351+390	60×45	+32	103	0.5
0352+825	50×45	−81	97	0.8
0418+148	90×40	+24	92	0.8
0429+174	81×41	+25	207	0.4
0529+013	99×46	+20	110	0.8
0638+357	53×44	+24	48	1.5
0732+237	81×43	+26	240	0.5
0817+710	50×44	+35	120	0.4
0819+082	106×41	+22	70	0.7
0824+355[a]	63×46	+30	563	0.1
0905+420	52×40	+47	90	0.75
1003+174	77×43	+23	199	0.4
1010+287	68×43	+29	181	0.3
1011+496	48×41	+83	189	0.3
1058+245	68×42	+26	85	0.75
1143+446	48×42	+88	140	0.6
1150+095	94×41	+23	294	0.25
1211+334	62×42	+35	680	0.15
1212+177	76×43	+25	239	0.5
1233+539	49×41	+56	98	0.7
1241+735	56×48	+14	139	0.5
1317+199	67×43	+28	86	0.7
1342+341	50×46	+22	83	1.0
1504+105	92×40	+25	133	0.5
1628+216	72×42	+29	128	0.4
1638+124	89×41	+26	630	0.3
1642+054	110×41	+23	132	0.3
1722+562	59×45	+20	145	0.4
1744+260	62×42	+29	121	0.5
1801+036	104×42	+21	60	0.7
1812+412	66×43	+31	357	0.25
1857+630	53×43	+30	78	0.6
1928+681	52×42	+25	95	1.0
2101+664	51×43	+37	74	0.75
2112+312	58×44	+30	126	0.5
2150+124	88×41	+24	181	0.25
2151+174	78×42	+28	165	0.4
2201+044	135×42	+20	267	0.8
2205+389	52×46	+12	107	0.7
2210+085	108×40	+24	141	0.9
2247+140	90×39	+26	390	0.5
2345+113	86×41	+24	133	0.4

[a] Quality control source.

imaging of compact components for these simple structures. Three sources (B0352+825, B1744+260 and B1801+036) did produce acceptable maps which enabled us to rule them out as gravitational lens candidates. B0352+825 was also followed up with the VLBA in the second session on the basis that it still could be a CSO. The maps are shown in Fig. 4 and the models fitted in Table 5. The map parameters of the three sources together with the parameters for the two quality control sources are presented in Table 6.

4 RESULTS

The final maps of the 50 sources observed with MERLIN and the VLBA are shown in Fig. 4. We now give a brief description of each of the 55 sources in our complete sample and the morphological classification adopted. For brevity, whenever we refer to 'the VLA map' we mean the 8.4-GHz A-array image obtained from a single snapshot during the JVAS and CLASS surveys. Whenever we refer to a MERLIN map or model without specifying the frequency we are referring to the 5-GHz results presented in Fig. 4 and Table 3. Unless we refer to this possibility explicitly, the reader should assume that the data show no evidence for multiple imaging of milliarcsec-sized cores with separations in the range 90–300 mas.

References for the optical identifications and redshifts obtained from the literature are listed in Table 1. Since we do not have redshifts for the majority of our sources we are unable to calculate their linear sizes and thus to differentiate between CSOs ($\lesssim$ 1 kpc) and MSOs (1–15 kpc). Note, however, that for $H_0 = 75$ km s^{-1} Mpc^{-1} and $q_0 = 0.5$ the boundary between CSO and MSO corresponds to an angular size of 211 mas (1 kpc) at $z = 0.5$. Most of our optically unidentified sources which are classified as CSO/MSOs are likely to fall within a factor of 3 of the 1-kpc boundary.

B0046+316: The source is identified with a Seyfert II galaxy at $z = 0.015$. It was observed and mapped partly as a quality control for comparison with the map presented by Unger et al. (1984) – their Fig. 1(c). Both maps (and the model in Table 3) show a bright compact central component flanked by weaker, more extended components. The overall extent of ~300 mas corresponds to ~90 pc and hence we classify it as a low-luminosity CSO with a bright core.

B0112+518: The VLA map shows a double with separation 0.65 arcsec. The MERLIN map also shows two discrete components, the appearance of which suggests that this may be a core–jet source. However modelling reveals that the putative core in the south is resolved (FWHM 56 mas) and hence the source could be a CSO/MSO with an undetected central component. Observations at higher resolution are required to settle the classification.

B0116+319: This compact double (also known as 4C31.04) in a bright elliptical galaxy at $z = 0.0592$ was observed partly as quality control for comparison with the 327-MHz map presented by Wrobel & Simon (1986) – their fig. 2(a). At 327 MHz the SE/NW flux ratio is 0.57 but at 5 GHz it is 2.9 showing that the NW component has a much steeper spectrum than the SE. A recent VLBA map at 1.34 GHz (Conway 1997) shows conclusively that these components are the twin lobes of a CSO, exhibiting complex H I absorption across both lobes and a faint core.

B0127+145: The MERLIN map and model reveal a core plus bending jet structure. The VLA map shows extended structure to the N and E of the compact component confirming the reality of the diffuse component in the MERLIN map.

B0205+722: The object is tentatively identified with a 22-mag galaxy at $z = 0.895$ (Vermeulen et al. 1996 and R. C. Vermeulen, private communication). The VLA map confirms the reality of the diffuse emission to the NW of the central compact core in the MERLIN map and model. The more intense compact component to the W of the core is revealed as a bright jet with no mas substructure by the CJ2 survey VLBI observations (Taylor et al. 1994). If the redshift is correct the overall angular size of ~600 mas corresponds to a linear size of ~3 kpc and hence this source can be classified as an MSO with a bright core.

Table 3. The models fitted to the MERLIN 5-GHz data. For each Gaussian component S is the flux density, r and θ describe the separation vector from the origin, a is the major axis, b/a is the axial ratio and Φ is the position angle of elongation.

Source	S (mJy)	r (mas)	θ (°)	a (mas)	b/a	Φ (°)
B0046+316	168	0.0	0.0	25.1	0.63	6.1
	42	133.1	173.5	46.1	0.71	37.5
	19	127.0	−34.3	46.7	0.53	44.8
B0112+518	45	0.0	0.0	56.1	0.70	89.7
	92	166.7	−12.3	136.6	0.57	−29.5
	35	756.1	−19.7	286.8	0.36	−23.7
B0116+319	773	0.0	0.0	22.6	0.49	10.3
	215	22.8	−66.4	38.3	0.54	27.9
	27	48.6	−39.1	4.8	1.00	0.0
	134	80.6	−61.0	66.8	0.00	10.6
	290	79.3	−71.0	36.6	0.45	64.6
B0127+145	358	0.0	0.0	16.9	0.37	−0.6
	51	168	103	66.7	0.00	70.8
	54	146.4	76.4	163.1	0.23	19.1
	18	491.0	20.2	252.0	0.00	54.1
B0205+722	278	0.0	0.0	12.5	0.82	72.5
	65	122.7	−103.8	32.0	0.65	48.8
	61	188.1	28.2	157.6	0.80	−11.0
B0225+187	106	0.0	0.0	26.6	0.54	−5.9
	35	208.0	120.3	25.3	0.39	−32.1
B0233+434	108	0.0	0.0	12.3	0.86	62.5
	63	120.0	−90.7	13.2	0.16	64.6
B0345+085	56	0.0	0.0	15.8	0.00	−54.4
	30	53.5	176.7	116.5	0.52	−5.2
	19	96.3	177.6	68.7	0.18	13.5
	6	287.7	−110.4	89.4	0.62	44.3
B0351+390	105	0.0	0.0	13.7	0.00	43.3
	12	445.8	46.9	107.6	0.89	23.1
B0352+825	81	0.0	0.0	17.5	0.00	84.4
	74	43.7	138.0	30.8	0.22	−57.6
B0418+148	25	0.0	0.0	25.9	0.00	77.6
	129	68.8	30.3	58.9	0.57	42.0
	34	117.6	−4.4	112.6	0.00	−74.1
	22	321.6	−50.3	328.5	0.19	32.0
B0429+174	216	0.0	0.0	16.1	0.51	16.0
	31	131.9	−55.8	62.4	0.64	7.6
	17	429.3	−106.8	431.7	0.25	42.4
B0529+013	125	0.0	0.0	30.9	0.58	−26.2
	12	45.2	139.4	55.3	0.00	−65.7
	12	180.6	134.8	42.0	0.64	45.1
B0638+357	44	0.0	0.0	16.6	0.00	−35.7
	38	60.5	124.4	153.3	0.07	−55.6
	46	204.5	−37.1	48.2	0.62	−66.2
	67	162.2	129.0	49.2	0.80	−58.0
B0732+237	272	0.0	0.0	18.4	0.11	−69.4
	29	53.4	−123.5	60.6	0.38	−3.9
	181	177.7	−59.3	33.6	0.49	32.4
	19	180.8	−40.8	77.0	0.00	−20.7
B0817+710	168	0.0	0.0	27.1	0.77	−76.9
	87	178.9	−63.3	56.3	0.45	−79.3
	38	231.8	−66.4	31.7	0.91	38.1
B0819+082	112	0.0	0.0	63.9	0.63	32.5
	67	178.2	−162.8	126.1	0.38	17.5
B0824+355	584	0.0	0.0	15.4	0.67	87.4
	175	106.6	69.0	117.1	0.40	87.9
	35	385.6	95.6	264.8	0.33	−44.9
B0905+420	91	0.0	0.0	4.5	0.75	77.1
	31	93.1	−133.3	65.2	0.37	72.6
B1003+174	211	0.0	0.0	30.5	0.43	43.0
	107	68.4	−114.2	69.7	0.50	−79.8
	48	300.5	−37.6	125.0	0.32	36.2
B1010+287	187	0.0	0.0	20.2	0.55	39.1
	92	53.7	−21.2	29.4	0.54	−25.3
B1011+496	173	0.0	0.0	12.3	0.00	47.7
	136	82.7	−99.0	69.9	0.46	74.4
	18	239.7	−99.2	110.9	0.00	34.9
B1058+245	92	0.0	0.0	62.4	0.35	19.3
	86	46.7	−160.6	102.6	0.52	31.2
	19	850.1	−156.9	314.0	0.30	−59.9
B1143+446	125	0.0	0.0	20.6	0.00	84.4
	73	44.1	90.6	89.0	0.30	−88.2
	17	205.3	57.5	57.1	0.00	−89.9
B1150+095	284	0.0	0.0	21.9	0.00	40.4
	54	78.3	15.5	69.6	0.56	23.7
	60	125.0	−10.8	34.4	0.50	−81.0
B1211+334	673	0.0	0.0	7.8	0.01	42.1
	30	12.5	43.4	21.1	0.00	22.0
	7	160.5	−85.7	70.8	0.00	−46.3
	91	301.9	−71.4	21.4	0.86	−12.8
B1212+177	266	0.0	0.0	34.0	0.14	49.4
	87	103.1	−128.5	50.9	0.27	72.0
B1233+539	140	0.0	0.0	34.7	0.94	−43.2
	94	71.0	−54.7	36.8	0.94	24.8
	26	234.6	−55.9	78.3	0.24	−72.6
B1241+735	138	0.0	0.0	5.3	0.26	24.5
	31	292.2	−29.7	96.7	0.42	−7.5
B1317+199	57	0.0	0.0	18.1	0.51	−50.7
	39	110.7	100.6	49.8	0.72	26.7
	140	189.5	95.7	54.1	0.68	36.2
	10	225.9	68.6	91.6	0.00	−14.2
	39	259.5	69.2	242.3	0.15	21.5
B1342+341	71	0.0	0.0	14.1	0.33	59.5
	33	29.8	2.9	25.8	0.53	−16.5
	14	192.7	−21.0	119.5	0.17	26.2

Table 3 – *continued*

Table 3 – *continued*

Source	S (mJy)	r (mas)	θ (°)	a (mas)	b/a	Φ (°)
B1504+105	142	0.0	0.0	24.9	0.00	−71.0
	41	74.1	99.9	94.7	0.00	−55.8
	19	110.8	99.5	76.4	0.00	18.8
B1628+216	143	0.0	0.0	26.4	0.48	59.0
	12	140.7	−111.3	57.2	0.33	31.7
	15	223.5	−104.6	67.1	0.45	35.2
	25	739.2	61.2	405.6	0.48	45.6
B1638+124	684	0.0	0.0	13.5	0.75	6.7
	304	144.4	−49.8	45.1	0.62	−19.1
B1642+054	132	0.0	0.0	19.4	0.26	30.2
	67	212.3	51.9	127.0	0.51	43.7
	18	778.7	42.5	185.7	0.51	70.8
	30	1137.5	35.1	672.0	0.20	49.5
B1722+562	146	0.0	0.0	8.1	0.00	66.1
	24	319.1	49.3	53.8	0.53	−9.7
	13	681.2	34.3	221.0	0.10	68.7
B1744+260	134	0.0	0.0	14.1	0.43	−22.3
	76	110.4	126.9	34.4	0.78	−21.9
	9	167.5	134.8	120.7	0.00	−16.0
B1801+036	65	0.0	0.0	25.1	0.57	10.6
	25	101.0	121.4	32.4	0.56	81.3
	7	433.3	−35.9	224.8	0.00	−14.8
	18	435.6	124.0	658.6	0.30	−57.6
B1812+412	290	0.0	0.0	12.1	0.00	−19.5
	117	16.5	56.8	59.0	0.10	66.0
	45	177.0	49.8	107.3	0.56	45.4
	42	234.2	−0.4	393.0	0.15	−72.3
	19	241.3	−39.6	158.7	0.19	−70.7
B1857+630	79	0.0	0.0	14.9	0.00	65.3
	21	52.2	63.5	38.2	0.51	2.4
	42	120.3	57.8	72.8	0.62	72.3
	6	281.3	80.6	101.7	0.00	−35.8
B1928+681	116	0.0	0.0	38.9	0.75	−18.2
	89	51.9	−33.5	116.0	0.07	−36.6
	30	67.5	−43.4	53.6	0.00	19.5
	103	128.6	−32.1	43.8	0.73	9.7
	7	338.5	44.5	143.9	0.00	−6.0
B2101+664	75	0.0	0.0	13.3	0.23	17.4
	22	294.8	−109.2	32.1	0.88	−34.6
	5	366.7	−115.4	35.2	0.43	−65.0
B2112+312	111	0.0	0.0	20.4	0.16	−12.3
	48	22.7	101.0	46.8	0.00	−36.6
	30	70.2	96.9	49.7	0.13	−84.6
	14	125.0	106.5	57.4	0.00	−4.7
	9	187.4	120.1	54.1	0.24	−36.8
B2150+124	186	0.0	0.0	14.5	0.61	2.3
	44	89.3	−47.1	98.2	0.50	10.7
	24	384.8	−142.0	246.8	0.15	7.1
B2151+174	140	0.0	0.0	16.7	0.00	−23.3
	36	16.1	8.0	49.6	0.00	6.1
	22	85.0	2.3	55.4	0.36	8.4
	3	186.0	178.9	122.6	0.00	39.5
B2201+044	324	0.0	0.0	32.1	0.29	−44.4
	27	200.6	−49.6	92.7	0.35	12.1
B2205+389	150	0.0	0.0	35.3	0.75	−81.0
	7	146.8	0.5	62.4	0.00	−1.4
	48	207.4	−3.8	36.9	0.10	20.5
	53	316.7	−3.9	113.4	0.50	−9.7
B2210+085	132	0.0	0.0	26.0	0.17	−17.7
	46	88.2	160.8	66.7	0.42	38.5
B2247+140	477	0.0	0.0	34.6	0.62	53.1
	296	79.3	−118.3	82.6	0.41	33.5
	117	181.0	−141.2	51.3	0.45	−7.5
	315	193.8	−154.1	133.2	0.72	−34.5
B2345+113	124	0.0	0.0	18.6	0.00	−26.2
	29	88.5	−169.7	104.4	0.00	−52.5
	33	14.5	98.8	125.8	0.11	21.6
	9	133.9	24.2	142.5	0.29	40.7

B0218+357 (not mapped by us): This is a gravitational lens system with a 335-mas separation (Patnaik et al. 1993). This is the only lens amongst our sample, although it is outside our 90–300 mas search range.

B0225+187: The MERLIN map and model show a compact double, the components of which are about equal in size (~26 mas). This source was therefore followed up with the VLBA as a lens candidate. The full-resolution VLBA map shows that both components are well resolved and outer-edge brightened. The VLBA map at 10 mas resolution is also shown which reveals further extensions to each component. There must, however, be additional low-brightness emission not revealed in this latter map since it only accounts for about half the total flux density of the source. The VLBA results show that the source does not consist of two images of a mas-scale core and it is most naturally interpreted as a CSO/MSO with an undetected core. By combining these MERLIN and VLBA data we improve the coverage of the *uv*-plane. The resultant map (not shown) does not support the lensing hypothesis as there are some extended components in the line between the two main compact components that are better ascribed to a jet. Nevertheless we cannot unequivocally rule out the possibility that the two components are images of an extended (~ 10 mas scale) background source. Further observations to trace out the details of the low-brightness emission are required to determine the correct classification of B0225+187.

B0233+434: The MERLIN map and model reveal a compact double with virtually unresolved components (~12 mas). It was therefore observed with the VLBA as a promising lens candidate. The VLBA map shows that both components are well resolved and are outer-edge brightened; this is therefore not a doubly imaged core but almost certainly a CSO/MSO with an unidentified core. The spectral turn-over at ~200 MHz (Fig. A1) is consistent with synchrotron self-absorption in components ~10 mas in size. Although the source is optically unidentified its angular extent of only 120 mas means it is most likely to be a CSO.

B0345+085: The MERLIN map suggests a core with a southerly pointing jet; this is supported by model fitting. The VLA map shows an extension to the west which confirms the weak component in the MERLIN map and suggests that the jet bends through 90°.

Table 4. The parameters for the VLBA 5-GHz maps.

source B1950.0	beam (mas)	PA (°)	map peak (mJy beam^{-1})	1st contour (3σ) (%)
0225+187	3.9×2.0	−8	6	6
0225+187	10×10	0	24	3
0233+434	3.0×1.5	+11	10	3
0352+825	2.4×2.1	−37	24	1.5
0732+237	3×3[a]	0	34	2
0817+710	4×4[a]	0	13	3.5
1010+287	2.9×1.5	−1	36	1.5
1211+334	2.8×1.5	+2	407	0.07
1212+177	3.2×1.7	−3	9	6.5
1504+105	4×4[a]	0	9	7.5
1857+630	2.4×2.2	+36	35	0.9
1928+681	2.2×2.1	+60	36	1
2151+174	3.2×1.8	−7	115	0.25

[a]The map shown was convolved with a restoring beam other than the natural beam.

Table 5. The models fitted to the MERLIN 22-GHz data. For each Gaussian component S is the flux density, r and θ describe the separation vector from the origin, a is the major axis, b/a is the axial ratio and Φ is the position angle of elongation.

Source	S (mJy)	r (mas)	θ (°)	a (mas)	b/a	Φ (°)
B0352+825	78	0.0	0.0	2.8	0.76	9.9
	21	21.1	−43.5	10.8	0.00	−84.9
B0732+237	96	0.0	0.0	7.8	0.86	44.1
	44	178.6	−60.4	19.2	0.37	35.7
B1211+334	208	0.0	0.0	4.0	0.07	46.7
	15	286.7	−72.4	12.2	0.00	−39.6
B1744+260	261	0.0	0.0	2.8	0.82	60.3
	37	98.6	129.8	22.7	0.00	−36.3
B1801+036	97	0.0	0.0	7.9	0.00	−23.3
	23	113.6	127.3	38.6	0.00	−31.5

Table 6. The parameters for the MERLIN 22-GHz maps.

source B1950.0	beam (mas)	PA (°)	map peak (mJy beam^{-1})	1st contour (3σ) (%)
0352+825	11×10	+21	67	4
0732+237	16×8	+24	63	3
1211+334	14×8	+37	195	1.3
1744+260	12×9	+23	247	1.5
1801+036	26×8	+22	86	3

B0351+390: The MERLIN map and model show a compact component plus a diffuse component ~450 mas to the NE. The VLA map also shows an extension ~500 mas to the NE suggesting that the structure is that of a core plus diffuse jet.

B0352+825: The optical identification is with a bright 17-mag galaxy. The MERLIN map and model are consistent with a compact double (separation ~ 44 mas) with barely resolved components. The source was therefore observed with MERLIN at 22 GHz and the VLBA as a lens candidate. The MERLIN 22-GHz map and model also show a double source but the SE component is the stronger of the two whereas at 5 GHz the NW is the stronger. This marked spectral difference ($\alpha_{SE} \sim 0$, $\alpha_{NW} \sim 1$) strongly suggests that we are not looking at two lensed images and that the active core of the compact double is towards the SE. This is confirmed by the VLBA map which clearly shows the core with a bent jet towards the NW. This map also shows diffuse emission to the SE which is not seen in the lower resolution MERLIN maps. Although its redshift is unknown it is likely to be $z \sim 0.1$; hence we can confidently classify this object as a CSO with a bright radio core since its linear size must be $\ll$1 kpc.

B0418+148: The MERLIN map and model suggest that this is a core plus sharply bent jet source, with the most compact component at the SW end of the central component in the map. The VLA map also shows an extension to the NW, approximately in the position of the low-level contours in the MERLIN map ~400 mas from the putative core.

B0429+174: The MERLIN map and model shows a core plus jet. The VLA map shows a weak extension ~600 mas to the SW in the same position as the weak outer components on the MERLIN map. The jet therefore bends through ~90° on kpc scales.

B0529+013: The MERLIN map and model suggest a core plus jet with the most compact component in the NW. The VLA map also shows a slight extension to the SE confirming the weak component in the MERLIN map. There is a small possibility, from model fitting, that the core is lensed but if so it would be on <50 mas scales. This candidate can hence be rejected as a 90–300 mas lensed system.

B0638+357: The MERLIN map shows a compact triple but the model reveals that while the central component is barely resolved (~16 mas) the outer components are well resolved (~50 mas); these are therefore not multiple images of a compact core. The overall extent of the source is ~400 mas and hence it is most likely to be a bright-core MSO.

B0732+237: The MERLIN map and model show a compact double with each component showing slight extensions perpendicular to the line of separation. This source was therefore followed up both with MERLIN at 22 GHz and with the VLBA as a lens candidate. The MERLIN 22-GHz data do not support the lensing hypothesis since modelling suggests that the weaker NW component is more extended than the stronger SE one; in addition the flux ratio between the two components is 1.5 at 5 GHz and 2.1 at 22 GHz. The VLBA map shows both components to be well resolved with neither containing a dominant compact component and the source is most naturally interpreted as a faint-core CSO/MSO. The higher brightness region of the NW component looks like a twin hotspot, however it must have additional low-brightness emission associated with it which is not shown in this map. The SW component has a bright hotspot towards the inner edge of diffuse lobe-like emission. This component must also have further low–brightness emission not seen in the map.

B0817+710: The MERLIN map shows what appears to be an unresolved core plus jet but model fitting indicates a triple source with all components significantly resolved—more suggestive of an MSO. This source was observed with the VLBA and the map shows that the latter interpretation is likely to be the correct one. The bright SE component in the MERLIN map has the form of an outer-edge brightened lobe while the 'jet-like' NW feature in the MERLIN map is diffuse leading us to suspect that this source is a faint-core MSO. Observations at different frequencies are required to confirm

this classification. The present data do, however, rule out the possibility of multiple imaging of a milliarcsec-scale core.

B0819+082: The MERLIN map shows an apparent core plus jet but model fitting indicates a double source with well-resolved components; multiple imaging of a mas core is therefore ruled out. Thus, like B0817+710, we suspect that this is a faint core MSO rather than a core–jet but higher resolution observations are required to confirm this classification.

B0821+394 (not mapped by us): This source has been mapped in the CJ1 VLBI surveys by Xu et al. (1995) and Thakkar et al. (1995). It consists of a core with compact knot ~ 200 mas distant.

B0824+355: The optical identification is with a QSO at $z = 2.249$ (Allington-Smith et al. 1988). This source was observed by MERLIN partly as a quality control for comparison with the 5-GHz CJ2 VLBI survey map (Henstock et al. 1995); the CJ2 map confirms the core plus jet structure at position angle 70° seen in the MERLIN map and model out to ~100 mas. The MERLIN map then shows a further extension of the jet to the E at position angle 90°. A 5-GHz VLA map presented by Naundorf et al. (1992) shows a faint 1.8-arcsec counterjet at position angle −120° with an outer hotspot. VLA maps at 6 and 20 cm by Taylor et al. (1996) show an extended resolved feature 14 arcsec away from the core at position angle 115° and if this feature is physically associated then the overall extent of the source is ~ 80 kpc and it would be classified as an LSO. If the structure is not associated then the overall extent is ~ 11 kpc and the source can be classified as an MSO dominated by a bright core and jet.

B0831+557 (not mapped by us): The dominant structure of this 11-arcsec double (Whyborn et al. 1985) is on a < 300 mas scale. However, VLBI observations show this structure to consist of a central core plus a ~ 150 mas jet (Pearson & Readhead 1988; Polatidis et al. 1995).

B0905+420: The MERLIN map and model show a clear core plus jet structure. There is a hint that the jet bends through ~80° about 120 mas from the core.

B0916+718 (not mapped by us): A core with a ~ 500 mas jet (King 1995).

B1003+174: The MERLIN maps and model suggest a core plus bent jet structure. An extension on the VLA map confirms the reality of the diffuse component to the NW in the MERLIN map.

B1010+287: The MERLIN map and model suggest a compact double, the components of which have roughly similar sizes and hence this source was followed up with the VLBA as a lens candidate. The components are well resolved in the VLBA map and their elongations agree with those suggested by the MERLIN model. The overall appearance of the source at high resolution does not suggest multiple imaging of a compact core and in particular the southern component is clearly more diffuse than the northern. It is most likely that the source is a faint-core CSO, indeed the VLBA map shows a hint of a central core. It could, however, be a core plus jet with the core at the northernmost end. Further high-resolution imaging is required to confirm our CSO classification.

B1011+496: The optical identification is with a 15.5-mag BSO at $z = 0.2$, if the object is a member of the cluster Abell 950 (Puchnarewicz et al. 1992; Laurent-Muehleisen et al. 1993). It is also classified as a BL Lac object (Véron-Cetty & Véron 1993). The MERLIN maps and model show a clear core plus jet. The VLA map shows that the jet extends ~1 arcsec to the W as is suggested by the weak outer components in the MERLIN map. Machalski & Condon (1983) show the structure to be larger than 5 arcsec on a VLA 1.4-GHz map.

B1058+245: The VLA map shows a double source with the secondary component 0.9 arcsec at position angle 170° from the stronger northern component; the N component has a weak extension to the E. The MERLIN map shows that this discrete southern component is well resolved while the northern appears to be a core plus jet. The weak extension to E on the VLA map is not seen and must be diffuse. Modelling shows, however, that the 'core' is well resolved (62 mas). Thus, rather than being a core–jet, it is possible that this is an MSO with an undetected core. However, this would be surprising since the fractional polarization (11 per cent) is the highest among the sources in our sample.

B1143+446: The MERLIN map and model suggest a core plus bent jet structure. The VLA map shows a faint extension of the jet towards the N out to ~0.4 arcsec.

B1150+095: The optical identification is a QSO at $z = 0.698$ (Wills & Wills 1976). The MERLIN map and model suggest a core plus bent jet structure. The VLA map shows a faint extension towards position angle −15° and the hint of a secondary about 5 arcsec away. A 15-GHz VLA map (Bogers et al. 1994) shows a weak secondary 5 arcsec away but towards south.

B1211+334: The optical identification is a QSO at $z = 1.598$ (Wills & Wills 1976). The VLA map shows a compact double structure with the brightest component to the E. The MERLIN map shows the same basic configuration but with a faint central component; the model suggests that the E component is more compact than the W and that the central component is resolved. Nevertheless the structure was sufficiently intriguing that the source was observed with MERLIN at 22 GHz and with the VLBA as a possible lens candidate. The MERLIN 22-GHz map is dominated by the E component, which the model shows is very compact (< 4 mas); there is just a hint of the W component in the map but this is not required by the model. The VLBA map confirms that the E component is very compact, and if the brightest component is the active core then there are two antiparallel jets extended at position angles 40° and −140°. Alternatively it could be a one-sided core–jet with the active, rising spectrum, core at the NE end. The W component, not resolved by the MERLIN beam, consists of a diffuse component, elongated perpendicular to the line joining it with the core, and a faint component ~35 mas to the SW. The faint central component in the MERLIN map is not visible. Clear spectral and morphological differences rule this source out as a lens but observations with higher surface brightness sensitivity are needed to look for faint emission around and between the components in order to make a reliable morphological classification.

B1212+177: The MERLIN map apparently shows a core plus jet but the model suggests that the bright NE component is resolved and elongated; nevertheless this source was observed with the VLBA as a possible lens candidate. The VLBA map confirms the essentials of the MERLIN model. Both components are diffuse with the NE one highly elongated and the one on the SW largely resolved out. We classify the source as a faint core CSO/MSO although with an angular size of ~100 mas it is more likely to be a CSO.

B1233+539: The MERLIN map and model show a source in which all the components are significantly resolved and hence it cannot consist of multiple images of a compact core. The VLA map shows no additional structure on arcsec scales. Higher resolution observations are required to classify the structure but we suspect that this is a faint-core CSO/MSO which may be associated with the cluster Abell, Corwin & Olowin 1568 (unknown redshift; e.g. Abell, Corwin & Olowin 1989).

B1241+735: The optical identification is with a bright 17-mag galaxy at $z = 0.075$ (Marchã et al. 1996). The MERLIN map and model show a core together with an extended component at position

angle −30°. The VLA map shows a jet extending out to ∼0.9 arcsec at the same position angle, thus the extended component in the MERLIN map is almost certainly a knot in a diffuse jet.

B1317+199: The MERLIN map shows a source with an ∼80° bend in the middle at the position of the brightest component. The model reveals that this bright component is well resolved (∼100 mas) while the component at the W end is very compact (< 20 mas); we conclude that this is a core plus bent jet. The VLA map shows a diffuse extension to the N which must be the continuation of the jet; there is also a faint extension to the S.

B1342+341: The MERLIN map and model show a core plus diffuse components to the NW. The VLA map shows an extension in at position angle −20° and also a weak discrete component 0.8 arcsec to SW. Almost certainly the source has a diffuse jet which bends through ∼100°.

B1504+105: This source cannot be unambiguously optically identified as on the plate we see a blend of two objects with an oval aspect. The identification is probably the southernmost 16th-magnitude component. The MERLIN map shows a compact double and although the model suggests that the W component is significantly more compact than the E the source was followed up with the VLBA as a lens candidate. The VLBA map shows that the E component is almost resolved out while the W is elongated and outer-edge brightened. We classify the source as a faint-core CSO/MSO although it is likely to be a CSO since its angular extent is only 110 mas.

B1628+216: The optical identification of this source was not possible as it lies very close to a 4th magnitude star. The MERLIN map and model show a compact central core plus extended structure on both sides. To the W is a knotty jet with resolved subcomponents while to the NE is a region of diffuse emission. The VLA map shows a discrete secondary 0.8 arcsec from the core at position angle 80° confirming the reality of this diffuse emission. We classify the source as an MSO with a bright core.

B1638+124: This source is an empty field on POSS but Stickel & Kühr (1996b) and Stickel et al. (1996) identify it as a 21.8-mag compact galaxy at $z = 1.152$. It has an optical companion only 3 arcsec away at the same position angle as the radio secondary component in relation to the primary. The MERLIN map agrees with the VLA map in showing a compact double but the MERLIN model reveals that the SE component is much more compact (< 15 mas) than the NW component (> 45 mas). The source is therefore almost certainly a core plus jet.

B1642+054: The MERLIN map and model reveal a compact core plus extended well-resolved jet. The VLA map confirms that the jet extends for ∼2 arcsec.

B1722+562: The MERLIN map and model show a compact core plus two well-resolved components to the NE; this is almost certainly a core plus jet source. The VLA map is consistent with the MERLIN map but shows no additional structure on arcsec scales.

B1744+260: The MERLIN map and model show a compact core with a jet-like structure to the SE; the 'jet' contains barely resolved (35 mas) substructure. The source was observed with MERLIN at 22 GHz and the data show that the jet is almost resolved out while the core is < 3 mas in diameter; the core has a sharply rising spectrum between 5 GHz and 22 GHz.

B1801+036: The MERLIN map shows a compact double source (separation ∼100 mas) flanked by diffuse outer components; the latter are also visible in the VLA map, giving an overall size of ∼1.2 arcsec. The MERLIN model reveals that the flux density of the NW core component is 2.6 times that of the SE and yet it is more compact than the SE suggesting that they are not lensed images. Nevertheless it was followed up with MERLIN at 22 GHz. Only the NW component is clearly detected at 22 GHz while the SE component is almost resolved out. The spectrum of the NW component is rising from 5 to 22 GHz and hence this is the active core. Overall the source can be classified as an MSO with a bright core.

B1812+412: The MERLIN map and model show a core plus bent jet. The VLA map is consistent with the MERLIN map but also shows a weak component ∼2 arcsec at position angle −10°. In the CJ2 VLBI maps (Henstock et al. 1995) the jet starts at position angle 90° hence the jet bends quasi-continuously from mas to arcsec scales.

B1857+630: The MERLIN map and model show a core plus jet with barely resolved substructure in the jet; the source was therefore followed up with the VLBA. The VLBA map shows that the jet in the MERLIN map is well resolved, except within ∼20 mas of the core. The VLA map shows a hint of an extension at position angle 100° consistent with the jet bending, as suggested in the MERLIN map.

B1928+681: The MERLIN map shows a compact double or triple structure while model fitting required five components and even then the fit was far from perfect. Since the classification remained uncertain the source was followed up with the VLBA. The VLBA map shows a bright core with a sinuous jet to the SE. There is diffuse emission to the NW of the core more clearly revealed in a tapered map. This is a CSO/MSO with a bright core.

B1947+677 (not mapped by us): This source has been followed up with MERLIN and the VLBA as part of another CLASS lens campaign. It is a bright-core MSO with an overall extent of ∼ 500 mas (Sykes 1997).

B2101+664: The MERLIN map and model show an asymmetric core plus jet-like structure. The VLA map shows no additional structure on arcsec scales.

B2112+312: The MERLIN map and model strongly suggest an asymmetric core plus bending jet structure. The VLA map shows no additional structure on arcsec scales.

B2150+124: The MERLIN map and model show an asymmetric core plus sharply bent jet structure; the VLA map shows that the jet extends out to ∼0.8 arcsec.

B2151+174: The MERLIN map and model suggest that the primary component consists of a compact, but elongated, core at the southern end with more extended (∼50 mas) components towards the N. There is also a weak extended secondary component almost due south. Even though the model does not immediately suggest multiple imaging the source was followed up with the VLBA. The VLBA map is consistent with the MERLIN model but reveals that the elongated compact component consists of a core plus a *southerly pointing* jet; the component 16 mas to the N of the core in the MERLIN model is seen to be well resolved in the VLBA map while the component 85 mas to the N is diffuse at this resolution. The secondary component in the MERLIN map is resolved out by the VLBA. The radio source is coincident with a cD galaxy in the centre of the rich cluster Abell 2390 at a redshift of 0.231 (Le Borgne et al. 1991), associated with a gravitationally lensed arc and arclets (Pell o et al. 1991). The radio source is classified as a bright-core CSO, with a size of 300 mas or 0.9 kpc.

B2201+044: This source is identified with a nearby $z = 0.028$ BL Lac (eg. Laurent-Muehleisen et al. 1993). Low-resolution VLA maps show that the radio source is highly asymmetric and is dominated by a core and jet at position angle $\sim -75°$ which extends over ∼ 5 arcmin (Laurent-Muehleisen et al. 1993). The

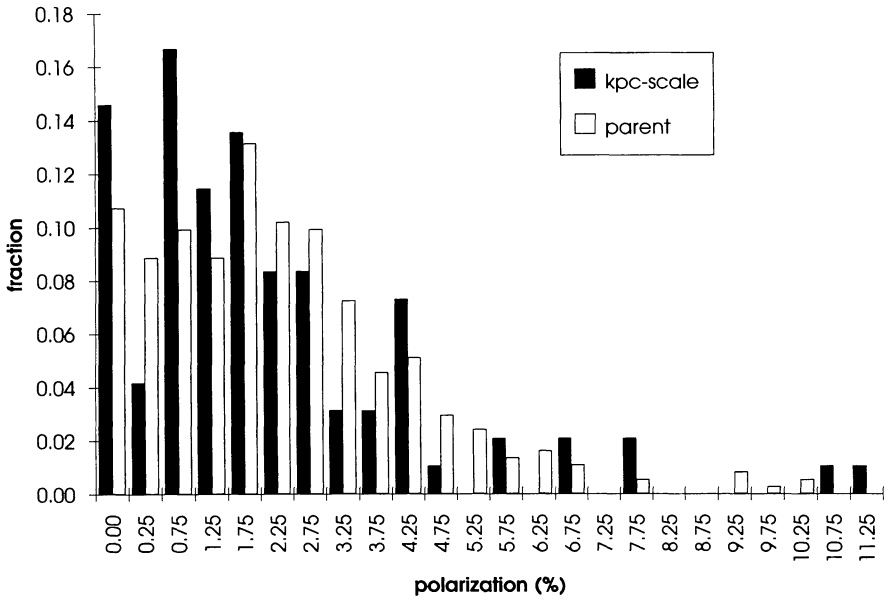

Figure 5. The percentage polarization distribution for 48 JVAS sources of the sample with kpc-scale structure compared with the distribution of a representative subsample of the parent sample. They are statistically indistinguishable and have a mean of ~2 per cent.

MERLIN map and model show the core and a weak feature in the jet.

B2205+389: The MERLIN map and model show a partially resolved core plus a jet extending over ~400 mas; the VLA map shows that the jet extends out to ~600 mas.

B2210+085: The MERLIN map and model show a core plus resolved jet-like extension at position angle 160°. The VLA map also shows a weak extension at position angle 160° plus amorphous emission ~1 arcsec to the SW.

B2247+140: The MERLIN map and model reveal a partially resolved core plus bent jet structure.

B2345+113: The MERLIN map and model show a compact core with a jet-like feature at position angle −170° and a bent jet starting at position angle 24°. The VLA map shows faint emission several hundred mas away on both sides of the core at positon angles ~100° and −45°. This all strongly suggests that the source is a bright-core CSO/MSO with an S-shaped symmetry but higher resolution observations are required to confirm the classification.

5 DISCUSSION

The MERLIN 5-GHz observations provided a very effective 'filter' that immediately ruled out about three-quarters of our candidates as gravitational lens systems. The subsequent VLBA and MERLIN 22-GHz observations enabled us to rule out the remaining lens candidates, apart from B0225+187 which, while most likely a CSO/MSO, is not definitely ruled out as being lensed. Apart from this weak case, there are no high-magnification gravitational lens systems with separations in the range 90–300 mas in our parent sample of 1665 objects. We shall discuss the implications of this result in detail in Augusto & Wilkinson (in preparation).

5.1 The statistical properties of flat-spectrum radio sources with kpc-scale structure

We now briefly compare the statistical properties of flat-spectrum radio sources with kpc-scale structure with the 1665-object 'parent' sample.

5.1.1 *Percentage polarization*

Polarization information is available from the JVAS 8.4-GHz observations (with the exception of the candidate B2201+044) but not for the CLASS sample. Hence, we can examine the polarization properties of 48 candidates. The distribution of 8.4-GHz percentage polarization is shown in Fig. 5. The parent and candidate distributions are indistinguishable and both have an average polarization of ~ 2 per cent.

5.1.2 *Spectral index*

The spectral index distributions shown in Fig. 6 reveal that about two-thirds of the objects in the kpc-scale sample have spectral indexes close to the cut-off at $\alpha_{1.4}^{4.85} = 0.5$; the mean spectral index for this sample is $\alpha_{1.4}^{4.85} \simeq 0.3$ (see also Table 1), compared with 0.0 for the parent sample. The fact that our objects are selected to have extended structure on the scale of ~ 100 mas is clearly responsible for this difference.

5.1.3 *Optical identifications*

The property that most distinguishes the sources with kpc-scale structure from the parent sample is the distribution of optical identifications on the POSS plates – see Table 1. The identifications we list in this table were made by eye with the help of APM (Cambridge Automatic Plate Measurement of POSS plates) for positional accuracy only. We classified the sources 'as seen', i.e. blue or red and when fuzzy they were called galaxies. Empty fields (EF) were defined as those radio sources where no object is seen on POSS within a 5 arcsec radius of the radio position.

Fig. 7 summarizes the identifications and shows that the 55 sources with kpc-scale structure are drawn from a different

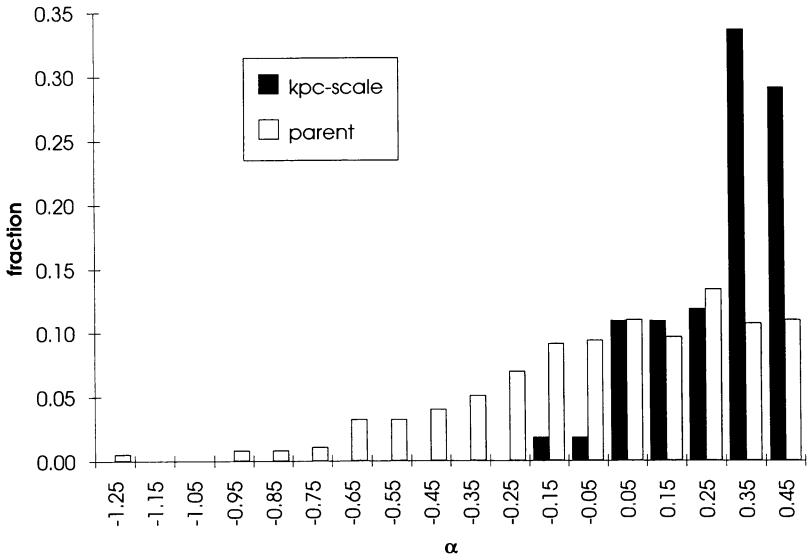

Figure 6. The spectral index distribution ($\alpha_{1.4}^{4.85}$) for the 55 flat-spectrum radio sources with kpc–structure compared with the distribution for a representative subsample drawn from the parent sample. The distributions clearly differ and the mean spectral index for the parent sample is 0.0 while that for the kpc-scale sample is 0.3.

population from that of the parent sample. While the fraction of EFs and RSOs is about the same in both samples, there are 40 per cent fewer BSOs in the kpc-scale source sample compared with the parent sample. The kpc-scale sample also has three times the fraction of galaxies seen in the parent sample.

5.1.4 *Radio classification*

In Table 1 we present our classification for the radio structures of all of our 55 sources with kpc-scale structure together with their optical identifications. We obtain two significant results.

(i) *Blue stellar objects are usually one-sided core–jets.* 14 out of 16 blue stellar objects are core plus one-sided jet sources. The nine blue/red stellar objects in our sample with relevant optical information in the literature are identified with seven QSOs and two BL Lacs. Four out of five sources with one-sided sharply (>90°) bent jets are blue stellar on POSS. Most likely these latter sources are QSOs since the other source with a sharply bent jet (B2247+140, red stellar on POSS) is a known QSO at $z = 0.237$.

(ii) *CSO/MSOs are usually in galaxies.* Seven out of 11 galaxies have CSO/MSO radio structures and 16 out of 21 of the probable CSO/MSOs are either galaxies or EFs, suggesting that they will mostly be identified with galaxies if we search deep enough in the optical.

In Table 7 we summarize the relative abundances of radio morphologies in the kpc-scale sample. A noteworthy result is that there are roughly as many CSO/MSOs with faint cores as with bright ones. In our 5-GHz maps/models, we define a CSO/MSO to have a faint core when the (sometimes putative) core is fainter than either of the lobes. Typically the core is 10–20 times fainter than the weakest lobe. We define a bright core as one the flux density of which is greater than at least one of the two lobes; typically, the core is 3–4 times stronger than the strongest of the two lobes. Using this definition, we have uncovered a new population of kpc-scale radio sources: bright-core CSO/MSO.

We can make a further test of the radio classifications by comparing the percentage polarization distributions in the CSO/MSO and core–jet populations. The results are shown in Fig. 8, which shows that the CSO/MSO population is concentrated towards lower values of percentage polarization than the core–jet population. This is consistent with what is known in the literature [e.g. Readhead et al. 1996a and references therein].

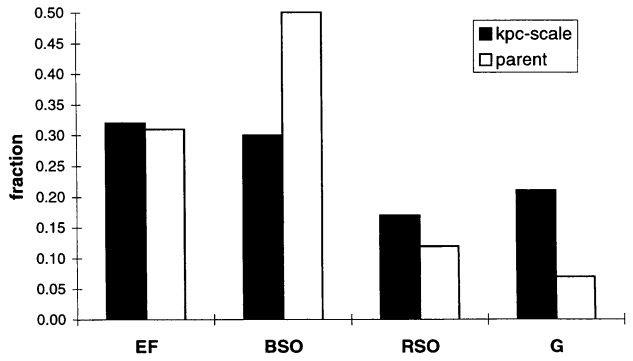

Figure 7. A comparison of the POSS optical identifications for the sample of 55 objects kpc-scale structure (represented here by 53 objects, as 1504+105 and 1628+216 have no identification) and a representative subsample of the parent sample. The identifications are: EF – empty field; R-BSO – red-blue stellar object; G – galaxy.

Table 7. The relative abundances of radio structure classifications in the subsample of 55 kpc-scale flat-spectrum sources. The 'other' bin includes a > 300 mas lens system and a large source (LSO).

morphology		abundance
CSO/MSO	bright core	20%
	faint core	22%
core–jets	nearly straight	31%
	sharply bent	24%
other		3%

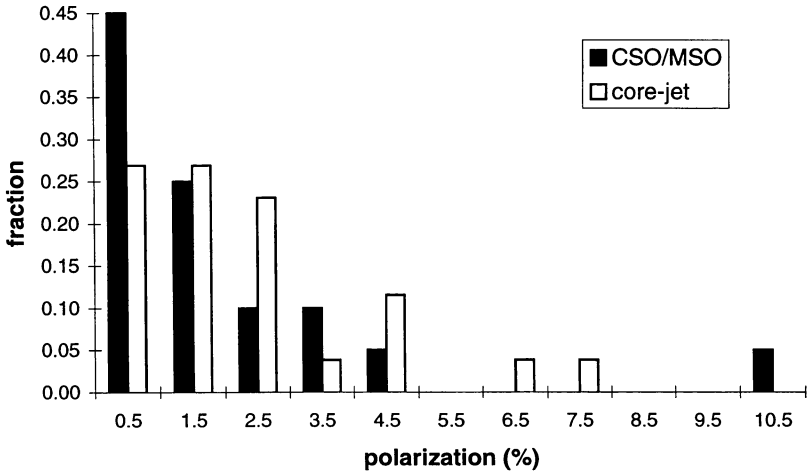

Figure 8. The percentage polarization distribution at 8.4 GHz of the two radio-identified populations in our sample of kpc-scale flat-spectrum objects: the CSO/MSO and the core–jet populations. The CSO/MSO population tends to have lower polarization than the core–jet population. One of the CSO/MSO candidates (B1058+245) has a considerably higher polarization (11 per cent) than any of the others which casts doubt on its classification.

Table 8. The 23 CSO/MSO candidates found in the kpc-scale sample. The linear size is calculated using $H_0 = 75$ km s^{-1} Mpc^{-1} and $q_0 = 0.5$. For sources marked with an asterisk the known redshift was used; for the remaining sources, without redshift information, we assume $z = 0.5$. CSOs at $z = 0.5$ will have angular sizes smaller than 211 mas.

source B1950.0	angular size (mas)	linear size (kpc)	classification
0046+316*	300	0.09	CSO
0112+518	650	3	MSO
0116+319*	75	0.08	CSO
0205+722*	600	3	MSO
0225+187	225	1	CSO
0233+434	120	0.6	CSO
0352+825*	44	$\sim 0.07^a$?	CSO
0638+357	400	2	MSO
0732+237	175	0.8	CSO
0817+710	225	1	CSO
0819+082	275	1	CSO
0824+355*	2000	11	MSO
1010+287	75	0.4	CSO
1058+245	900	4	MSO
1212+177	100	0.5	CSO
1233+539	240	1	CSO
1504+105	110	0.5	CSO
1628+216	800	4	MSO
1801+036	1200	6	MSO
1928+681	120	0.6	CSO
1947+677	500	2	MSO
2151+174*	300	0.9	CSO
2345+113	275	1	CSO

[a]A bright galaxy at $z \sim 0.1$?

We note finally that there is an apparent correlation between the brightness of a galaxy and the type of CSO/MSO seen at radio frequencies. Assuming for simplicity that all CSO/MSOs identified as EFs on POSS are faint galaxies, we find that bright-core CSO/MSOs preferentially reside in bright galaxies (easily seen on POSS) and faint-core CSO/MSOs lie preferentially in faint galaxies (close to or below the POSS limit). This is the equivalent to saying that cores are more dominant in the lower luminosity nearby CSO/MSOs.

5.2 The new CSOs/MSOs

Until now, the numbers and size distribution of flat-spectrum CSOs and MSOs with separations ~100 mas have been uncertain. Our search has found 23 new CSO/MSO candidates (see Table 8) out of a parent sample of 1665; thus there are only 1.4 per cent of flat-spectrum CSOs/MSOs in the angular size range ~90–300 mas (probable linear sizes ~0.5–1.5 kpc). There are significantly more CSOs on the ~ 10 mas scale. For example, Readhead et al. (1996a) suggest that between 5 and 10 per cent of CSOs are in high-frequency-selected radio surveys without regard to radio spectra. The number in the bona fide flat-spectrum CJF sample [Taylor et al. (1996), which uses the same $\alpha_{1.4}^{4.85}$ criterion that we used] remains to be determined but it is certainly > 5 per cent. To account for the relatively large numbers of tiny 'LSO precursors' in flux-density-limited samples, as compared with the numbers of evolved LSOs, the radio luminosity of symmetric sources must decrease by an order of magnitude or more as they expand (Fanti et al. 1995; Readhead et al. 1996a,b). Kaiser & Alexander (1997) have proposed a model in which the luminosity of double sources decreases proportionally to the square root of their size. Can we, therefore, explain the smaller number of CSO/MSOs in our sample compared with the numbers in the PR/CJ surveys by luminosity evolution? If, for example, Kaiser & Alexander's model applies to all angular size ranges, there could be a decrease in luminosity by a factor of about 3 in going from CSOs with a typical size of ~10 mas (PR/CJ) to those with a typical size of ~100 mas (present search). However, the flux density limit of the present search is about three times less than that of the PR/CJ surveys, and this compensates for the effect of decreased luminosity in our larger CSOs/MSOs.

We suggest instead that the small number of CSOs/MSOs in our sample is largely due to a selection effect. By observing flat-spectrum sources we are favouring objects dominated by compact (< 20 mas) components. Sources dominated by more extended components will have steep spectra and hence will not be included in the original JVAS/CLASS sample. Our results therefore show that there is not a significant population of kpc-sized CSOs/MSOs dominated by compact hotspots or bright cores. The greater fraction of CSOs dominated by compact hotspots found in the PR/CJ surveys indicates that compact CSO hotspots must expand as the

source itself gets larger – in other words, radio sources grow self-similarly. Essentially the same conclusion about the growth of GPS sources has been reached, using different arguments, by Snellen (1997).

6 SUMMARY

Radio interferometers can reveal the presence of structure in radio sources which are much smaller than the formal resolution limit. This ability allowed us to conduct a search on 90–300 mas scales on the JVAS/CLASS data base observed with the VLA A array at 8.4 GHz. The MERLIN 5-GHz snapshot observations proved to be a successful way for classifying a significant number of lens/CSO/MSO candidates in a small period of time. MERLIN 22-GHz snapshot observations were less successful mainly due to the much higher system noise. Nevertheless, if a source is strong enough, 22-GHz MERLIN data can still provide structural information for lens diagnosis. The VLBA was important for the final diagnosis, given its ability to provide reliable structural information on the remaining candidates with a few snapshots.

The results of our search of a large number of flat-spectrum sources shed new light on the flat-spectrum radio source population on kpc scales, a size range not studied systematically before. The implications of our results will be discussed fully in Augusto & Wilkinson (in preparation) but the main results can be simply stated. We found 23 new CSO/MSO candidates and our observations draw attention to a hitherto unrecognized population of flat-spectrum radio source: 'bright-core CSO/MSOs' which lie preferentially in optically brighter galaxies. The CSO/MSO results help to constrain evolutionary theories of symmetric radio sources. The fraction of $\sim$1 kpc scale CSO/MSOs is only 1.4 per cent of the population of flat-spectrum radio sources compared with the 5–10 per cent seen on the 100 pc scale. This means that the compact hotspots of CSOs must expand as the sources grow to become LSOs.

There are six multiply imaged arcsec-scale lens systems in JVAS, from a parent sample of about 2300 sources (King et al. 1998). Our search, among a starting sample of 1665 mainly JVAS sources, has not found any definite multiple gravitationally lensed cores in the angular range 90–300 mas (although B0225+187 remains a weak candidate). This suggests that there is a preferred scale for single galaxy lensing, of order 1 arcsec, corresponding to a preferred mass for the lens, of the order of 10^{11} $M_{\odot}$. The implication is that the optical depth to lensing with image separations in the range 90–300 mas is several times less than on arcsec scales. The vast population of $\sim 10^{8}$–10^{9} $M_{\odot}$ dwarf/faint galaxies is not contributing significantly to producing multiple imaging of background quasars.

ACKNOWLEDGMENTS

Pedro Augusto wishes to thank the Junta Nacional de Investigação Científica e Tecnológica for the grants Ciência/Praxis XXI BD 2623/93-RM and Praxis XXI BPD 9985/96. We thank Nectaria Gizani for an efficient tutorial on the basics of AIPS, Dave Shone for managing to 'unflip' some flipped maps, Neal Jackson for the scheduling programme for MERLIN snapshot observations and Tim Pearson for the FORTRAN program that produced the clear plots for the spectra of our sample. We also thank the MERLIN team for making *L*-band observations of three of our sources, and for the 'd' programmes and 'PIPELINE' data-reducing software. We thank the rest of the CLASS team for allowing us to use the results prior to publication.

MERLIN is operated by the University of Manchester on behalf of the Particle Physics and Astronomy Research Council. The VLBA is operated by the National Radio Astronomy Observatory (USA) as a National Facility. This search has made use of NED, the NASA/IPAC Extragalactic Database, the Parkes Catalogue (1990), published by the Australia Telescope National Facility, and Starlink distributed software.

REFERENCES

Abell G. O., Corwin H. G., Olowin R. P., 1989, ApJS, 70, 1
Allington-Smith J. R., Spinrad H., Djorgovski S., Liebert J., 1988, MNRAS, 234, 1091
Amirkhanyan V. R., Gorshkov A. G., Konnikova V. K., 1992a, SvA, 36, 115
Augusto P., 1996, PhD thesis, Univ. Manchester
Baars J. W. M., Genzel R., Pauliny-Toth I. I. K., Witzel A., 1977, A&A, 61, 99
Baldwin J. A., Burbidge E. M., Hazard C., Murdoch H. S., Robinson L. B., Wamper E. J., 1973, ApJ, 185, 739
Baldwin J. E., Boysen R. C., Hales S. E. G., Jennings J. E., Wagget P. C., Warner P. J., Wilson D. M. A., 1985, MNRAS, 217, 717
Biretta J. A., Zhou F., Owen F. N., 1995, ApJ, 447, 582
Bogers W. J., Hes R., Barthel P. D., Zensus J. A., 1994, A&AS, 105, 91
Bowen D. V., Blades J. C., Pettini M., 1995, ApJ, 448, 634
Browne I. W. A., Patnaik A. R., Walsh D., Wilkinson P. N., 1993, MNRAS, 263, L32
Browne I. W. A., Patnaik A. R., Wilkinson P. N., Wrobel J. M., 1998a, MNRAS, 293, 257
Browne I. W. A. et al., 1998b, in Bremer M., Jackson N., Perez-Fournon I., eds, Observational Cosmology with the new radio surveys. Kluwer, Dordrecht, p. 305
Burbidge G., Crowne A. H., 1979, ApJS, 40, 583
Condon J. J., Cotton W. D., Greisen E. W., Yin Q. F., Preley R. A., Taylor G. B., Broderick J. J., 1998, AJ, 115, 1693
Conway J. E., 1997, in Jackson N., Davis R. J., eds, High-Sensitivity Radio Astronomy. Cambridge Univ. Press, Cambridge, p. 153
Douglas J. N., Bash F. N., Bozyan F. A., Torrence G. W., Wolfe C., 1996, AJ, 111, 1945
Fanti C., Fanti R., Dallacasa D., Schilizzi R. T., Spencer R. E., Stanghellini C., 1995, A&A, 302, 317
Ficarra A., Grueff G., Tomassetti G., 1985, A&AS, 59, 255
Fukugita M., Turner E. L., 1996, ApJ, 460, L81
Fukugita M., Futamase T., Kasai M., Turner E. L., 1992, ApJ, 393, 3
Glazebrook K., Ellis R., Santiago B., Griffiths R., 1995, MNRAS, 275, L19
Green D. A., Riley J. M., 1995, MNRAS, 274, 324
Gregory P. C., Condon J. J., 1991, ApJS, 75, 1011
Griffiths R. E. et al., 1994, ApJ, 437, 67
Hales S. E. G., Baldwin J. E., Warner P. J., 1988, MNRAS, 234, 919
Hales S. E. G., Masson C. R., Warner P. J., Baldwin J. E., 1990, MNRAS, 246, 256
Hales S. E. G., Mayer C. J., Warner P. J., Baldwin J. E., 1991, MNRAS, 251, 46
Hales S. E. G., Masson C. R., Warner P. J., Baldwin J. E., Green D. A., 1993a, MNRAS, 262, 1057
Hales S. E. G., Baldwin J. E., Warner P. J., 1993b, MNRAS, 263, 25
Henstock D. R., Browne I. W. A., Wilkinson P. N., Taylor G. B., Vermeulen R. C., Pearson T. J., Readhead A. C. S., 1995, ApJS, 100, 1
Henstock D. R., Browne I. W. A., Wilkinson P. N., McMahon R. G., 1997, MNRAS, 290, 380
Hook I. M., McMahon R. G., Irwin M. J., Hazard C., 1996, MNRAS, 282, 1274
Im M., Casertano S., Griffiths R. E., Ratnatunga K. U., 1995, ApJ, 441, 494
Israel F. P., Seielstad G. A., Berge G. L., 1988, A&A, 189, 7
Kaiser C. R., Alexander P., 1997, MNRAS, 286, 215
King L. J., 1995, PhD thesis, Univ. Manchester
King L. J., Browne I. W. A., Marlow D. R., Patnaik A. R., Wilkinson P. N., 1998, MNRAS, in press
Kühr H., Witzel A., Pauliny-Toth I. I. K., Nauber U., 1981, A&AS, 45, 367

Laurent-Muehleisen S. A., Kollgaard R. I., Moellenbrock G. A., Feigelson E. D., 1993, AJ, 106, 875
Lawrence C. R., 1996, in Kochanek C., Hewitt J. N., eds, IAU Symp. 173. Astrophysical Applications of Gravitational Lensing, Kluwer, Drodrecht, p. 299
Le Borgne J.-F., Mathez G., Mellier Y., Pelló R., Sanahuja B., Soucail G., 1991, A&AS, 88, 133
Lilly S. J., Cowie L. L., Gardner J. P., 1991, ApJ, 369, 79
Machalski J., Condon J. J., 1983, AJ, 88, 1591
Machalski J., Inoue M., 1990, MNRAS, 243, 209
Machalski J., Magdziarz P., 1993, A&A, 267, 363
Marchã M. J. M., Browne I. W. A., Impey C. D., Smith P. S., 1996, MNRAS, 281, 425
Mobasher B., Rowan-Robinson A., Georgakakis A., Eaton N., 1996, MNRAS, 282, L7
Myers S. T., 1996, in Kochanek C., Hewitt J. N., eds, IAU Symp. 173 Astrophysical Applications of Gravitational Lensing. Kluwer, Dordrecht, p. 317
Naundorf C. E., Alexander P., Riley J. M., Eales S. A., 1992, MNRAS, 258, 647
Owen F. N., Spangler S. R., Cotton W. D., 1980, AJ, 85, 351
Patnaik A. R., Browne I. W. A., Wilkinson P. N., Wrobel J. M., 1992, MNRAS, 254, 655
Patnaik A. R., Browne I. W. A., King L. J., Muxlow T. W. B., Walsh D., Wilkinson P. N., 1993, MNRAS, 261, 435
Pearson T. J., 1991, BAAS, 23, 991
Pearson T. J., Readhead A. C. S., 1988, ApJ, 328, 114
Pelló R., Le Borgne J.-F., Soucail G., Mellier Y., Sanahuja B., 1991, ApJ, 366, 405
Polatidis A. G., 1993, PhD thesis, Univ. Manchester
Polatidis A. G., Wilkinson P. N., Xu W., Readhead A. C. S., Pearson T. J., Taylor G. B., Vermeulen R. C., 1995, ApJS, 98, 1
Price R., Gower A. C., Hutchings J. B., Talon S., Duncan D., Ross G., 1993, ApJS, 86, 365
Puchnarewicz E. M., Mason K. O., Córdova F. A., Kartje J., Branduardi-Raymont J., Mittaz J. P. D., Murdin P. G., Allington-Smith J., 1992, MNRAS, 256, 589
Readhead A. C. S., Taylor G. B., Xu W., Pearson T. J., Wilkinson P. N., Polatidis A. G., 1996a, ApJ, 460, 612
Roche N., Ratnatunga K., Griffiths R. E., Im M., Neuschaefer L., 1996, MNRAS, 282, 1247
Sargent W. L. W., 1973, ApJ, 182, L13
Sawicki M. J., Lin H., Yee H. K. C., 1997, AJ, 113, 1
Shepherd M. C., Pearson T. J., Taylor G. B., 1994, BAAS, 26, 987
Snellen I., 1997, PhD thesis, Univ. Leiden
Steppe H., Salter C. J., Chin R., Kreysa E., Brunswig W., Lobato-Pérez J., 1988, A&AS, 75, 317
Stickel M., Kühr H., 1996a, A&AS, 115, 1
Stickel M., Kühr H., 1996b, A&AS, 115, 11
Stickel M., Rieke G. H., Kühr H., Rieke M. J., 1996, ApJ, 468, 556
Sykes C. M., 1997, PhD thesis, Univ. Manchester
Taylor G. B., Vermeulen R. C., Pearson T. J., Readhead A. C. S., Henstock D. R., Browne I. W. A., Wilkinson P. N., 1994, ApJS, 95, 345
Taylor G. B., Vermeulen R. C., Readhead A. C. S., Pearson T. J., Henstock D. R., Wilkinson P. N., 1996, ApJS, 107, 37
Thakkar D. D., Xu W., Readhead A. C. S., Pearson T. J., Taylor G. B., Vermeulen R. C., Polatidis A. G., Wilkinson P. N., 1995, ApJS, 98, 33
Ulvestad J. S., Johnston K. J., Weiler K. W., 1983, ApJ, 266, 18
Unger S. W., Pedlar A., Neff S. G., de Bruyn A. G., 1984, MNRAS, 209, 15P
Unger S. W., Pedlar A., Booler R. V., Harrison B. A., 1986, MNRAS, 219, 387
Vermeulen R. C., Taylor G. B., Redhead A. C. S., Browne I. W. A., 1996, AJ, 111, 1013
Véron-Cetty M. P., Véron P., 1993, in ESO Scientific Report, 6th edn., No. 13
White R. L., Becker R. H., 1992, ApJS, 79, 331
Whyborn N. D., Browne I. W. A., Wilkinson P. N., Porcas R. W., Spinrad H., 1985, MNRAS, 214, 55
Wilkinson P. N., Polatidis A., Readhead A. C. S., Xu W., Person T. J., 1994, ApJ, 432, L87
Wilkinson P. N., Browne I. W. A., Patnaik A. R., Wrobel J. M., Sorathia B., 1998, MNRAS, in press
Williams R. E. et al., 1996, AJ, 112, 1335
Wills D., Wills B. J., 1976, ApJS, 31, 143
Wrobel J. M., Simon R. S., 1986, ApJ, 309, 593
Xu W., Readhead A. C. S., Pearson T. J., Polatidis A. G., Wilkinson P. N., 1995, ApJS, 99, 297
Zhang X., Zhen Y., Chen H., Wang S., 1993, A&AS, 99, 545

APPENDIX A: RADIO SPECTRA

In Fig. A1 we present the spectra for the 55 sources in the kpc-scale sample. The flux density data were obtained from the references listed in Table A1.

APPENDIX B: OTHER SOURCES

We also present the maps of eight sources that were mapped during our programme which are not formally in our sample because they either are dominated by large-scale structure (> 300 mas) or do not obey the strict spectral criterion. These maps are shown in Fig. B1 and the parameters in Table B1. A short discussion on each source follows.

B0219+428: This source is identified with a QSO with $z = 0.444$ (Bowen, Blades & Pettini 1995). The MERLIN data lacked Defford hence the the core–jet structure in the maps is not reliable in detail. The MERLIN map is, however, consistent with published results (cf. Price et al. 1993; Ulvestad, Johnston & Weiler 1983). The latter show that the source is very large (~ 100 arcsec), when all faint-jet emission is imaged.

B0813+020: The MERLIN map shows an elongated source at position angle 45°. Model fitting reveals three components, all well resolved (> 55 mas), and hence the source does not consist of multiple images of a compact core. It is likely that higher resolution observations would reveal this object to be an CSO or MSO. This source is variable at 5 GHz (Machalski & Magdziarz 1993) and hence it is likely to have a bright core.

B0945+664: This source is in the CJ1 VLBI sample (Polatidis et al. 1995) but did not produce fringes on baselines longer than a few hundred km (Polatidis 1993). VLA maps (Patnaik et al. 1992 and L. J. King, private communication) show a 0.78-arcsec double. Early MERLIN snapshot observations were interpreted as showing a core plus jet in the SW lobe (Polatidis 1993) but the current, better quality, map and model show that all subcomponents are well resolved and hence that this is an MSO with a faint core. This classification is consistent with the lack of compact structure detected in the CJ1 survey.

B1438+385: This source, known not to be lensed (Patnaik et al. 1992), was observed as a quality control to test the ability of our MERLIN snapshots to detect extended structure on arcsec scales. The MERLIN map and model show a compact core to the south with resolved knots ~6.9 arcsec to the north.

B1452+301: This object has been followed up with multifrequency VLA observations as an arcsec-scale lens candidate; it was found not to be lensed (King 1995). Our MERLIN map and model clarify the structure: the object is an MSO with a bright core.

B1545+497: The optical identification is with an RSO with $z = 0.7$ (Hook et al. 1996). The 8.4-GHz VLA map shows a slightly resolved 'core' with a faint jet-like structure extending about 3 arcsec at position angle −10°. The MERLIN map shows a single resolved component. The source was observed during the CJ2 VLBI survey by Henstock et al. (1995); a single weak (40 mJy) compact

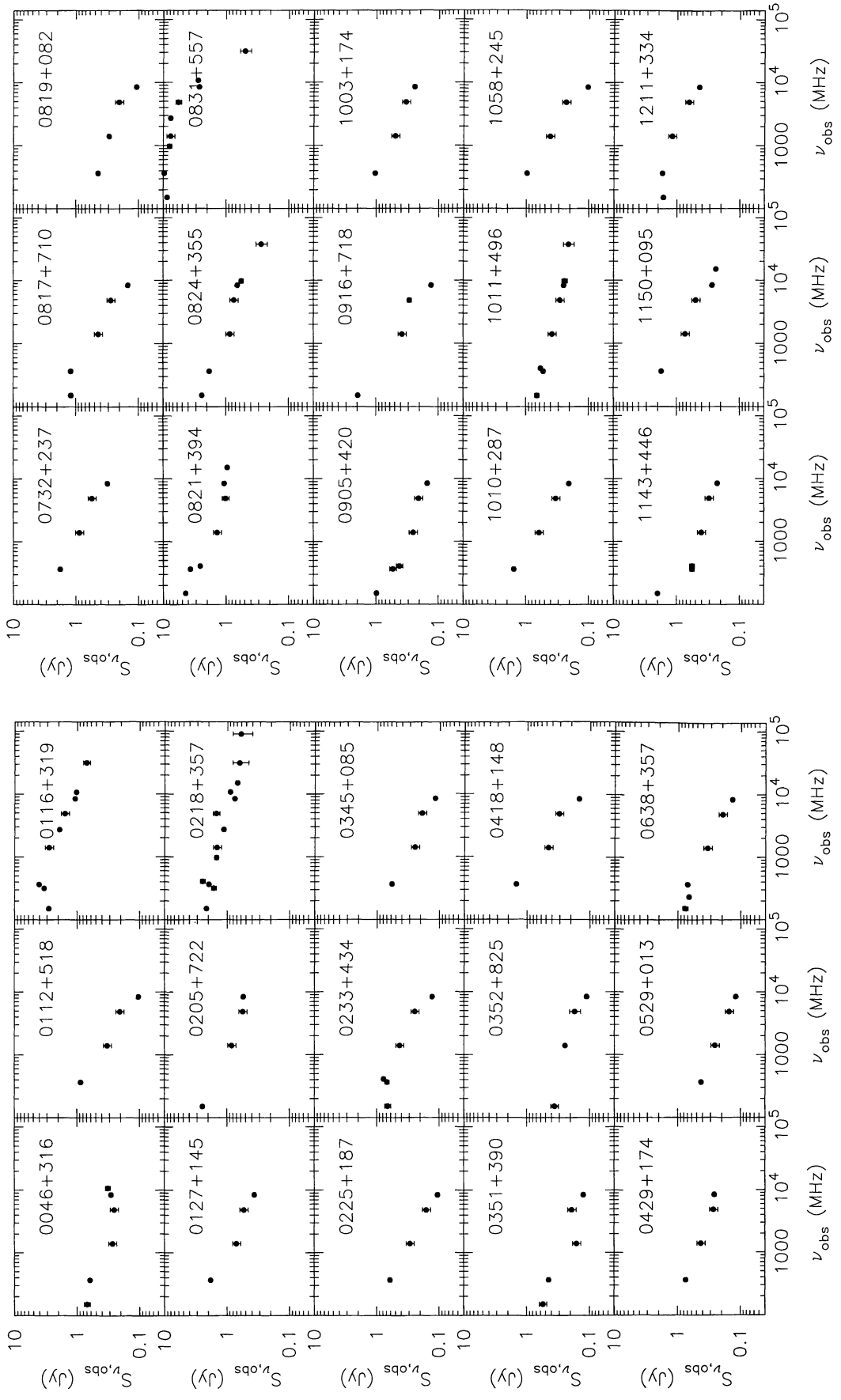

Figure A1. Radio spectra for the subsample of 55 kpc-scale flat-spectrum sources.

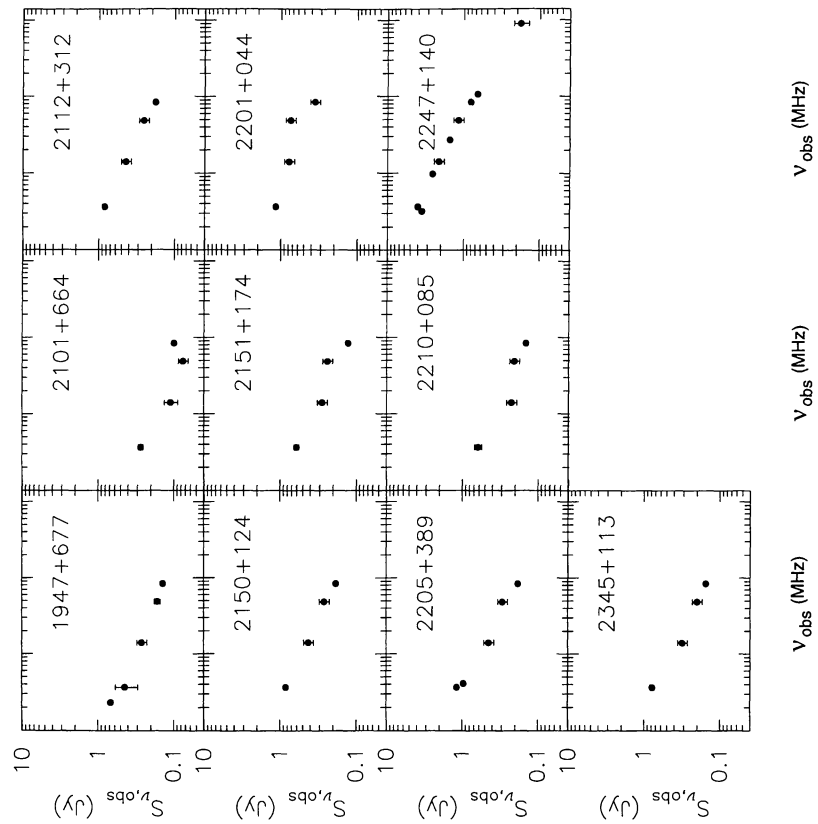

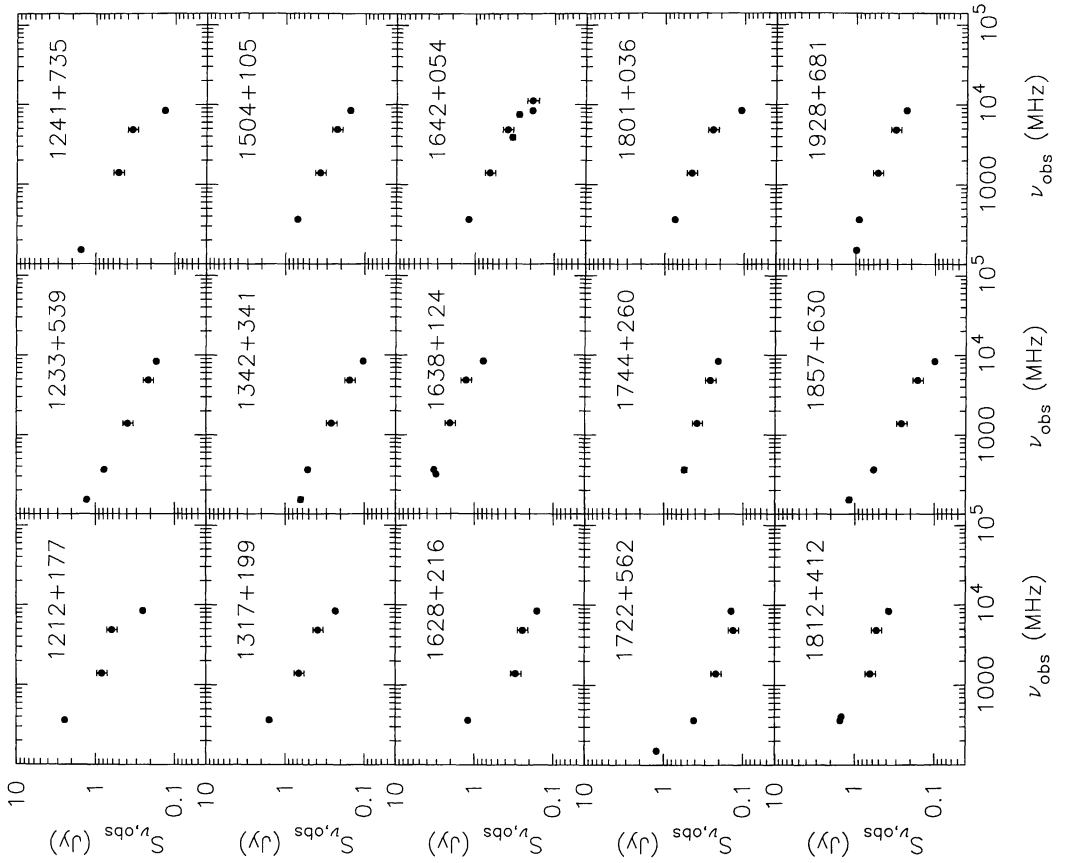

Figure A1 – *continued*

Table A1. The flux density catalogues/references used to produce the spectra of our 55 kpc-scale sources shown in Fig. A1. For some of the cases (in the 'comments' column) the flux density retrieved was for only one source.

frequency (MHz)	typical error	references	comments
151	50 mJy	Baldwin et al. (1985)	
151	50 mJy	Hales, Baldwin & Warner (1988)	
151	50 mJy	Hales et al. (1990,1991)	
151	75 mJy	Hales et al. (1993a)	
151	75 mJy	Hales et al. (1993b)	
232	30 mJy	Zhang et al. (1993)	B0638+357
318	150 mJy	Kühr et al. (1981)	
365	40 mJy	Douglas et al. (1996)	
408	220 mJy	Kühr et al. (1981)	B0218+357
408	50 mJy	Ficarra et al. (1985)	
408	3 per cent	Green & Riley (1995)	B1011+496
966	200 mJy	Kühr et al. (1981)	
1400	15 per cent	White & Becker (1992)	
1400	3 per cent	NVSS - Condon et al. (1998)	
1660	20 per cent	our MERLIN observations	B2101+664
2700	25 mJy	Kühr et al. (1981)	
3900	26 mJy	Amirkhanyan, Gorshkov & Konnikova (1992a)	B1642+054
4850	15 per cent	Gregory & Condon (1991)	
4995	20 per cent	our MERLIN observations	B0352+825
7500	18 mJy	Amirkhanyan, Gorshkov & Konnikova (1992a)	B1642+054
8400	5 per cent	JVAS/CLASS	
9800	20 per cent	Machalski & Inoue (1990)	
10700	25 mJy	Kühr et al. (1981)	
10700	29 mJy	Israel, Seielestad & Berge	B0046+316
11200	32 mJy	Amirkhanyan et al. (1992a)	B1642+054
15000		Bogers et al. (1994)	B1150+095
31400	200 mJy	Owen, Spangler & Cotton	
31400	150 mJy	Kühr et al. (1981)	
37500	25 per cent	Machalski & Inoue (1990)	
90000	40 mJy	Steppe et al. (1988)	B2247+140

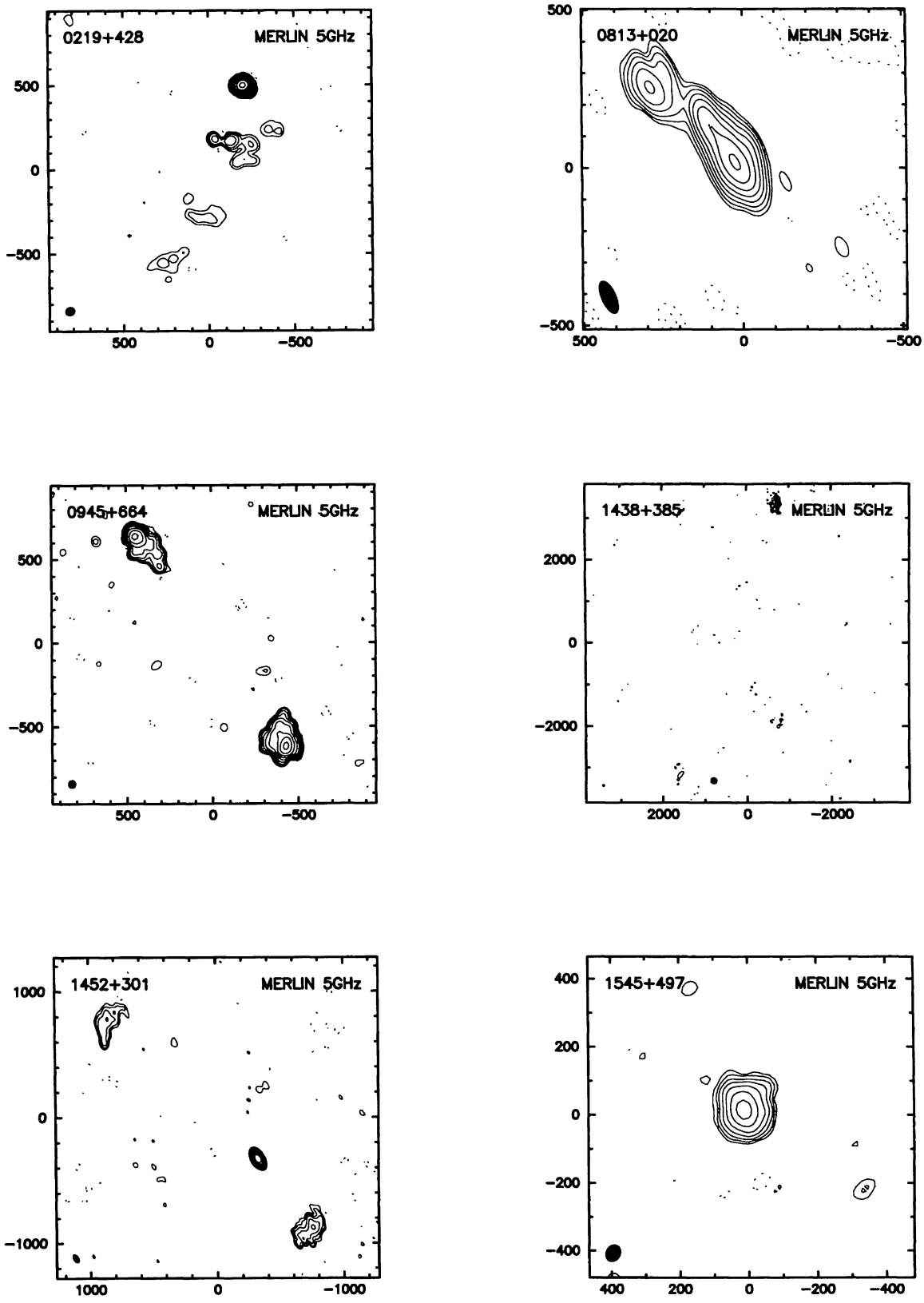

Figure B1. Maps of eight sources not in the sample of kpc-scale sources.

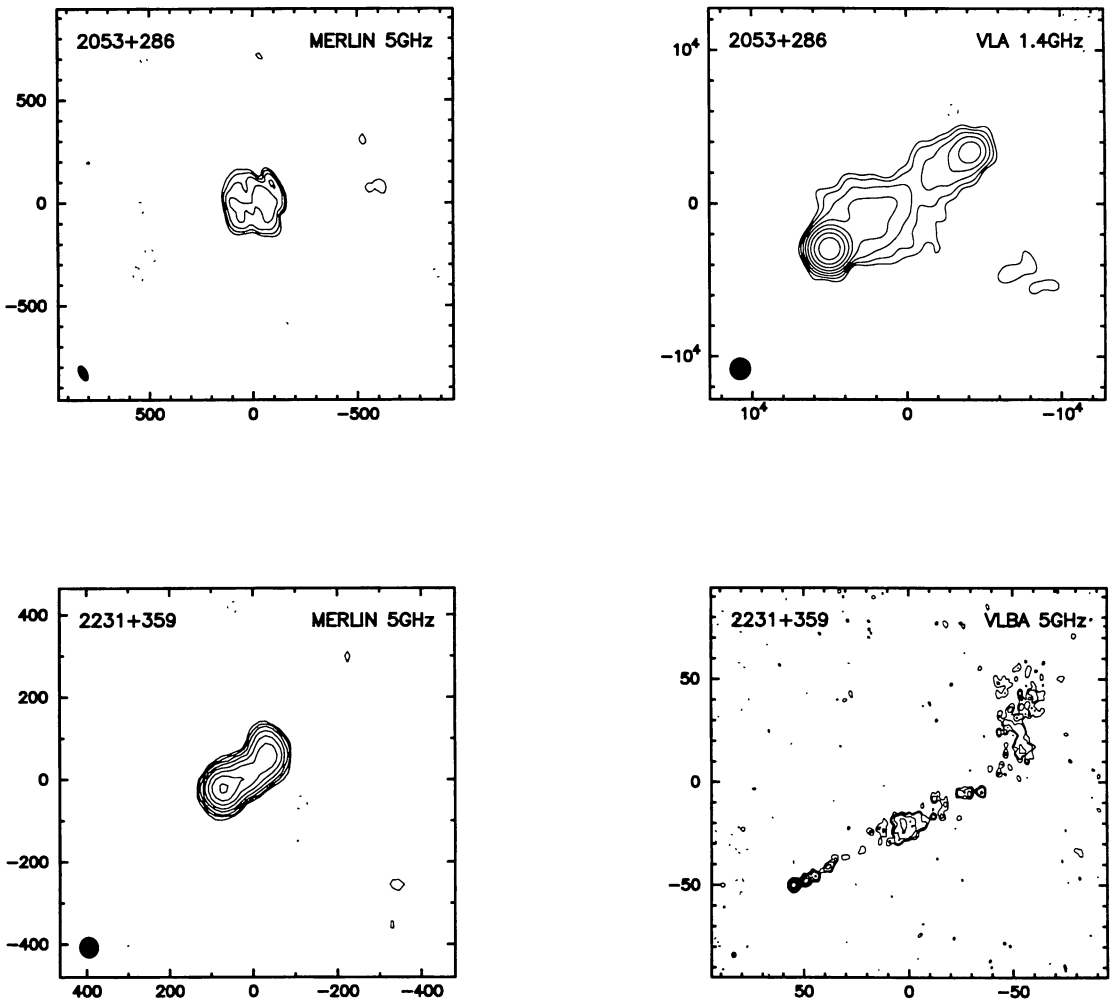

Figure B1 – *continued*

Table B1. The map parameters for eight sources not in the sample of kpc-scale sources.

source B1950.0	beam (mas)	P.A. (°)	map peak (mJy beam^{-1})	1st contour (3σ) (%)
		MERLIN 5 GHz		
0219+428	56×49	−68	650	0.15
0813+020	109×45	+23	102	0.7
0945+664	47×43	−2	274	0.3
1438+385	50×46	+40	576	0.25
1452+301	71×40	+31	164	0.4
1545+497	52×41	−26	150	1.0
2053+286	78×39	+26	11	7
2231+359	50×45	+4	74	0.7
		VLA 1.4 GHz		
2053+286	1420×1340	−4	371	0.4
		VLBA 5 GHz		
2231+359	2.6×2.0	+2	42	0.4

source only was detected. VLA 6- and 20-cm maps by Taylor et al. (1996) show that both our MERLIN map and the CJ2 VLBI map mapped the strongest southeastern lobe of a 6-arcsec LSO. The position angle of the large scale structure is −25°.

B2053+286: The MERLIN map indicates an amorphous source, very difficult to map, especially because we only had three snapshots of data. Subsequently, we observed this source with the VLA A array in the *L* band and found that the 'blob' in the MERLIN map is the E lobe of an LSO with LAS ∼ 10 arcsec. This VLA map is also presented.

B2231+359: The MERLIN map and model suggest a core plus resolved knotty jet; nevertheless the source was observed with the VLBA. The VLBA map is consistent with the MERLIN model and reveals an extensive jet with a transverse feature ∼50 mas from the core which has a strong morphological resemblance to knot A in the M87 jet (e.g. Biretta, Zhou & Owen 1995). In fact the entire jet is reminiscent of that in M87. The VLA map shows no additional structure on arcsec scales.

This paper has been typeset from a TEX/LATEX file prepared by the author.